Solar Sailing Asteroid Cycler

Time optimal heteroclinic-like connections between Sun-Earth L_2 and Sun-asteroid L_1 of asteroid 2001AE2

MSc Thesis

Olivier van Bon

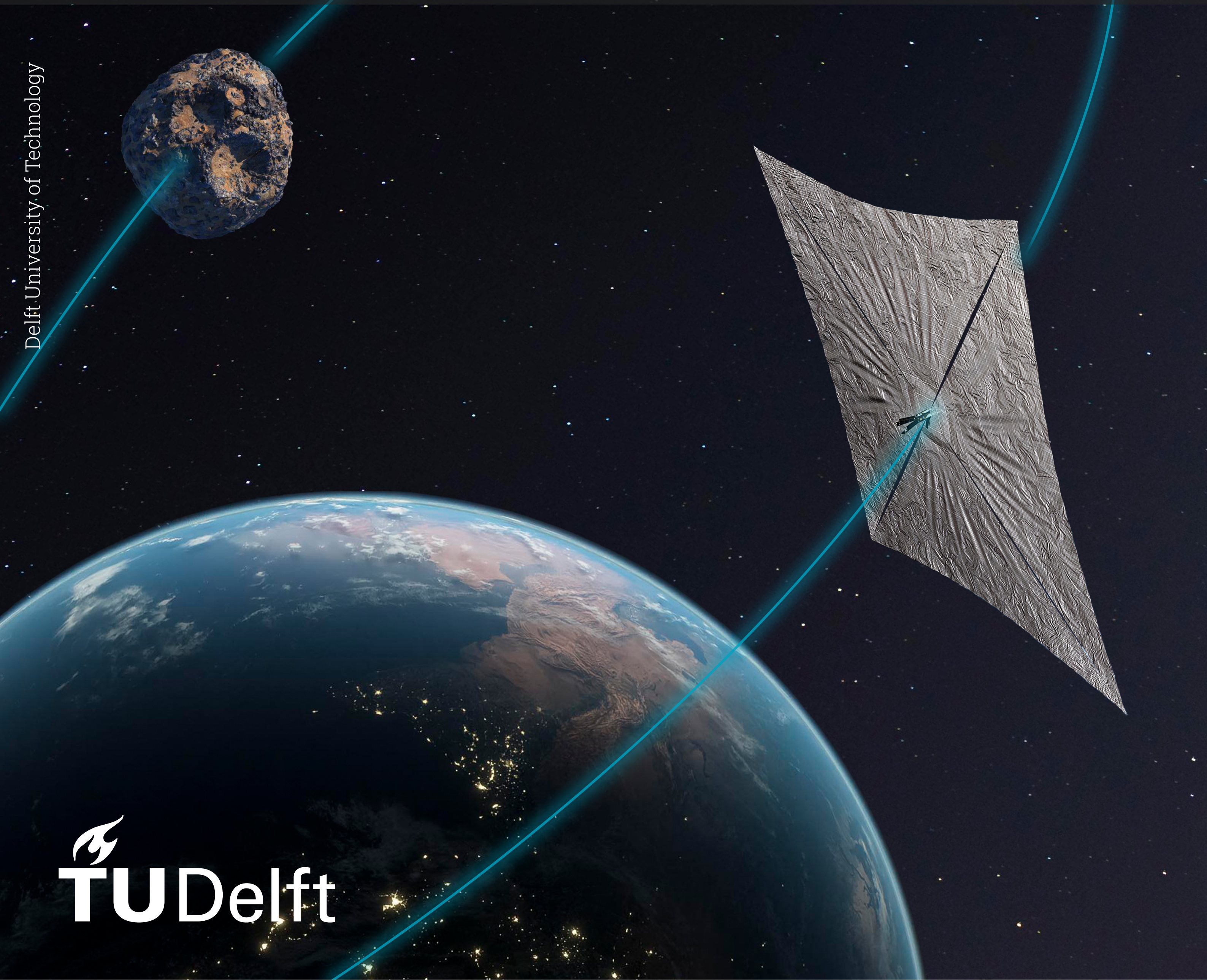

Delft University of Technology

TU Delft

Solar Sailing Asteroid Cycler

Time optimal heteroclinic-like connections between Sun-Earth L_2 and Sun-asteroid L_1 of asteroid 2001AE2

by

Olivier van Bon

to obtain the degree of Master of Science
at the Delft University of Technology,
to be defended publicly on Wednesday May 3rd, 2023 at 9:30 AM.

Student number:	1234567	
Thesis committee:	dr. W. van der Wal	TU Delft, Chair
	dr. M. J. Heiligers,	TU Delft, supervisor
	dr. B. Jyoti,	TU Delft, external examiner

An electronic version of this thesis is available at `http://repository.tudelft.nl/`.

Cover image	Credit
Solar Sail (LightSail 2)	Josh Spradling / The Planetary Society (CC BY-SA 3.0)
Earth	image: Freepik.com
Asteroid (Psyche)	NASA/JPL-Caltech/ASU

TU Delft

Preface

Please find in this report the efforts I have put into finishing my Master's degree in Aerospace Engineering. It investigates setting up a solar sail Earth-asteroid cycler.

Working on this project has not been the easiest throughout my studies (which one should not expect of a thesis project). The Covid-era has been a depressing one for many people in a variety of ways. For me it took away my opportunity to go to Tokyo for my internship at the last minute. When it was clear that expecting to start with my internship any time soon was futile, I was allowed to start working on my thesis project in late 2020. By this point I was excited to be able to do anything at all to get my study progress going again. But the ramifications Covid-19 had on society left me in a weird place, where I found it really difficult to stay motivated as the safety of the world around us was insecure and constantly changing.

It took me a while to get to this point, but I can now finally say I am happily done with this project. There are a lot of people who have helped me achieve this. Of course, I would first like to thank my supervisor, dr. Jeanette Heiligers, for her patience and guidance throughout this project.

Getting here was not always easy, but I am lucky to have had a lot of help and support from friends, family and most of all my girlfriend, Dayenne. Dayenne, you always ask me whether you do 'enough' to help me go through this process, but there was nothing more I wanted from you than to just stay by my side as I struggled along. You managed to do a whole lot more.

I'd also like to thank my younger brother Jasper and my sister Anna for being such caring siblings. Anna, I'd like to thank you specifically for helping me with the pretty cover image of this report, but also for your support over the years. I think because we struggle with similar things in life (both educational and personal matters), our bond has really grown over the years. Next, I'd like to thank my mother for always staying hopeful and caring in regards to my studies. You're always keen to remind me of the importance of education, which is now finally not necessary anymore! I'm done.

Finally, I'd like to thank all of the friends I've made during my studies, especially my old room mates from the Fourth Floor in Groningen and the Bagijnhof in Delft as well as my rowing team Fregadt. Last month I celebrated my birthday with some of you and it made me happier than I had been in a long time, reminding me of the value of friendship. I appreciate having you all in my life and I am glad that you stuck around with me over the past few years. Thank you.

Olivier van Bon
Delft, April 2023

Executive Summary

This thesis investigates the possibility of setting up an Earth-asteroid cycler to asteroid 2001AE2 using solar sail technology. Cyclers are spacecraft that repeatedly visit a set of destinations with minimal to no altering of the trajectories after each cycle. In this work, a cycler is investigated between the Sun-Earth Lagrange point 2 (SE – L2) and the Sun-asteroid Lagrange point 1 (Sa – L1) of asteroid 2001AE2. Lagrange points are gravitational equilibrium points in a three-body problem, where a spacecraft experiences balancing gravitational forces from two large bodies. The spacecraft could theoretically remain at rest here when undisturbed or it could orbit the co-rotating gravitational point. For context, the recently launched James Webb Space Telescope is in such an orbit around SE – L2. For simplicity, this thesis assumes the spacecraft to start from a stationary state at the Lagrange point, instead of from an orbit.

Cyclers can provide an effective logistical system for future long-duration space operations, such as crewed missions requiring continuous life support and resource utilization operations requiring cargo transport. This thesis work focuses on designing a cycler between Earth and asteroid 2001AE2 for a use-case like the latter. Asteroids vary widely in composition, but can contain large quantities of rare-Earth minerals. Asteroid mining operations can prove to not only be profitable, but also a way to increase sustainability by reducing mining on Earth.

To facilitate long-duration operations, this thesis employs solar sail technology. Unlike conventional propulsion methods, solar sails do not use any chemical or electrical propellant. By using a large, thin reflective membrane to reflect incoming Sunlight, a solar sail can generate thrust similar to how a sailboat on Earth is pushed forward by the wind. Because of this, they can be used indefinitely (or until the sail material degrades too much) and they are an ideal candidate for long-term operations. An ideal solar sail model with near-future technology levels is implemented with a lightness number (sail performance metric) of $\beta = 0.05$. For simplicity non-perfect sail properties are neglected, such as optical properties (e.g., non-perfect reflection) and billowing of the sail. These should be included in further research and can be expected to increase flight times by $\sim 10\%$.

To model the dynamics of the spacecraft, the thesis uses the circular restricted three-body problem (CR3BP) and the elliptic Hill problem (EH3BP). These dynamical models simulate the gravitational attraction of two large primary bodies to give a relatively accurate description of their influence on a third body. In this case, the CR3BP uses the Sun and Earth as the two primaries, while the EH3BP uses the Sun and the asteroid. These models are often used in preliminary trajectory design.

The cycler is designed by determining an outbound trajectory from SE – L2 to Sa – L1 and a following inbound trajectory from Sa – L1 back to SE – L2. The trajectories are searched for by using invariant manifolds. Invariant manifolds are trajectories that a spacecraft at a libration point would follow when given a small perturbation or along which a spacecraft can drift towards the libration point without requiring any propulsion. These trajectories are a natural product from the dynamical models and can be expanded by including the solar sail acceleration to create solar sail-assisted manifolds. These manifolds can be connected to form homoclinic connections (connecting a libration point to itself) or heteroclinic connections (connecting one libration point to another) within a three-body system (e.g., a Sun-planet system). Recent research has shown that heteroclinic connections can be found between different Sun-planet systems using solar sailing by connecting the CR3BP of one Sun-planet system to the CR3BP of another Sun-planet system. This thesis sets out to investigate the possibility of connecting the Sun-Earth CR3BP to the Sun-asteroid EH3BP of asteroid 2001AE2.

Finding a cycler between two Sun-planet systems is relatively simple, compared to finding a cycler between a Sun-planet system and a Sun-asteroid system. Sun-planet systems are in circular, coplanar orbits and therefore a cycle time can be found by using the synodic period. This is the time between consecutive oppositions or conjunctions (or any repeated relative configuration) of two bodies (e.g., two planets) orbiting a third (e.g., the Sun). After one or any multiple of synodic periods, the two bodies find themselves in the same relative configuriation (i.e., the angle between them is the same) and at the same distance from the Sun. However, many asteroids have a highly eccentric or inclined orbit. To illustrate this, more than $> 90\%$ of known NEAs have an eccentricity of $e > 0.2$ and more than half

have an inclination of $i \leq 10$deg. This requires the use of a different timing mechanism to ensure the absolute position of the primary bodies is the same at the start and end of a cycle. If only the same relative configuration is found at the end of a cycle (i.e., the angle between Earth and the asteroid is the same), the asteroid could be in a very different part of its orbit and the same set of trajectories cannot be reused. This thesis finds that the mean-motion resonance (MMR) of the two bodies is a good alternative to use in this case. While few asteroids exhibit a perfect MMR with Earth, many can be found with a minimal error. This means that in the time the asteroid completes an integer number of orbits, Earth completes a near-integer number of orbits with only a small error.

Using a genetic algorithm, connections between $SE - L2$ and $Sa - L1$ of 2001AE2 are searched for by connecting the CR3BP to the EH3BP. Because the EH3BP is only valid in close proximity to the asteroid (up to a few hundred kilometers) it is extended by a Sun-sail two-body problem (SS2BP). These trajectories use a constant sail orientation and are considered sub-optimal. An optimal trajectory would require knowing the ideal sail orientation throughout the entire trajectory to minimize the time of flight, meaning it is an infinite dimensional control problem. The connected trajectories found by the genetic algorithm are used as initial guess trajectories to seed the optimization software PSOPT. This pseudospectral collocation method uses Legendre-Chebyshev polynomials to transform the infinite dimensional control problem into a finite dimensional non-linear programming problem. This way a continuous control profile can be found that justifies the dynamical models and results in a time-optimal trajectory.

The resulting cycler is achievable within a cycle time of 11.04 years, with an outbound trajectory departing from $SE - L2$ at $01 - 03 - 2036$ and arriving at $Sa - L1$ at $02 - 04 - 2039$ and an inbound trajectory departing from $Sa - L1$ at $04 - 08 - 2043$ and arriving back at $SE - L2$ at $31 - 03 - 2046$. The dwelling time at $Sa - L1$ is 4.34 years and the dwelling time at $SE - L2$ is 351 days. These dwelling times are relatively long and can be further reduced by redoing the analysis with the synodic period instead of the MMR, since asteroid 2001AE2 has an orbit that is suitable for use with the synodic period. The trajectories are assumed time-optimal given the assumptions made in the work, but require further refining for non-ideal properties of the solar sail and other higher fidelity models.

Contents

Nomenclature **vii**

1 Introduction **1**
- 1.1 Research Context . . . 1
  - 1.1.1 Solar Sailing . . . 1
  - 1.1.2 Cyclers . . . 1
  - 1.1.3 Near-Earth Asteroids . . . 2
- 1.2 Research Objective and Questions . . . 3
- 1.3 Report Outline . . . 3

2 Journal Article **5**

3 Verification and Validation **39**
- 3.1 Dynamical Models . . . 39
  - 3.1.1 CR3BP . . . 39
  - 3.1.2 Hill problem . . . 39
- 3.2 Initial Guess Generation . . . 39
- 3.3 PSOPT Results . . . 41

4 Conclusions and Recommendations **43**
- 4.1 Review of Research Objective and Questions . . . 43
- 4.2 Recommendations . . . 46

References **47**

Nomenclature

Abbreviations

Abbreviation	Definition
AIAA	American Institute of Aeronautics and Astronautics
AU	Astronomical Unit
CR3BP	Circular Restricted Three-Body Problem
CR (subscript)	Related to the CR3BP
EH3BP	Elliptic Hill Three-Body Problem
EH (subscript)	Related to the EH3BP
MBA	Main Belt Asteroid
MMR	Mean motion resonance
NEA	Near-Earth Asteroid
NEO	Near-Earth Object
Sa – L1	Sun-asteroid Lagrange point 1
SE – L2	Sun-Earth Lagrange point 2
SS2BP	Sun-Sail Two-Body Problem
SS (subscript)	Related to the SS2BP

Symbols

Symbol	Definition	Unit
a	Semi-major axis	[km] or [AU]
$\boldsymbol{a}_s$	Solar-sail induced acceleration	[-]
$C(\hat{\boldsymbol{x}}, \hat{\boldsymbol{y}}, \hat{\boldsymbol{z}})$	Reference frame of CR3BP	[-]
D	Diameter (of asteroid)	[km]
e	Orbital eccentricity	[-]
E	Eccentric anomaly	[rad]
$E(\hat{\boldsymbol{X}}, \hat{\boldsymbol{Y}}, \hat{\boldsymbol{Z}})$	Reference frame of EH3BP	[-]
$\boldsymbol{g}$	Genetic algorithm chromosome	[-]
H	Absolute magnitude (of asteroid)	[-]
$H(\tilde{\boldsymbol{x}}_I, \tilde{\boldsymbol{y}}_I, \tilde{\boldsymbol{z}}_I)$	Heliocentric inertial frame (of SS2BP)	[-]
i	Orbital inclination	[-]
J	Objective function	[-]
m	Mass	[kg]
M	Mean anomaly	[rad]
n	Mean motion	[$\mathrm{y}^{-}1$]
$\hat{\boldsymbol{n}}$	Normal vector of solar sail	[-]
p_V	Albedo (visual band) of asteroid	[-]
ΔR	Position mismatch at connection point	[km]
$\mathbb{R}$	Rotation matrix	[-]
$\boldsymbol{R}$	Position vector of spacecraft in EH3BP	[-]
$\boldsymbol{r}$	Position vector of spacecraft in CR3BP	[-]
$\tilde{\boldsymbol{r}}$	Position vector of spacecraft in SS2BP	[km]
$\boldsymbol{s}$	State vector of spacecraft	[-]
s_v	Scale value in objective function	[-]
$\mathbb{T}$	Transformation matrix	[-]

Symbol	Definition	Unit
T	Orbital period	[y]
t	Time	[s] or [non-dim]
T_{cyc}	Cycle time	[y]
T_{syn}	Synodic period	[y]
T_p	Time of perihelion passage	[s]
U	Effective potential	[-]
$\boldsymbol{u}$	Control vector	[-]
V	Gratiational potential	[-]
α	Cone angle of the solar sail orientation	[rad]
β	Solar sail lightness number	[-]
δ	Clock angle of the solar sail orientation	[rad]
ϵ_{cyc}	MMR mismatch	[-]
λ_{CR}	Length scale of CR3BP	[km]
λ_{EH}	Length scale of EH3BP	[km]
μ	Gravitational parameter	[m^3s^{-2}]
μ_{CR}	Mass parameter of CR3BP	[-]
ν	Asteroid true anomaly	[rad]
ω_{ast}	Argument of periapsis of asteroid orbit	[rad]
ω	Rotation rate of CR3BP	[rad/s]
Ω	Rotation rate of EH3BP	[rad/s]
ρ	Sun-asteroid distance parameter in EH3BP	[-]
σ	Area-to-mass ratio	[g/m^2]
σ^*	Critical sail loading parameter	[g/m^2]
τ_{CR}	Time scale of CR3BP	[s]
τ_{EH}	Time scale of EH3BP	[s]
Φ	Centripetal potential	[-]

1
Introduction

This report describes the trajectory design of a solar sail asteroid cycler. Trajectory design is done using astrodynamics, which deals with describing the motion of the center of mass of a spacecraft [24]. In this work, specific trajectories are investigated between Earth and an asteroid. These trajectories are specifically designed in such a way that a repeatable round trip can be formed. This requires careful selection of the target asteroid, deliberate timing of the cycle phases and implementation of the correct dynamical models. By optimizing the trajectories with respect to their time of flight, the dwelling times at the asteroid and Earth can be maximized - which is desirable for mission operations. It is important to note that these trajectories are designed based on certain assumptions and should be considered as preliminary trajectories that showcase the future potential of solar sail asteroid cyclers.

1.1. Research Context

1.1.1. Solar Sailing

Recent years have shown innovative alternatives to conventional propulsion methods in the field of aerospace engineering. Similar to how the automobile industry sees a shift from combustion engines towards electric propulsion, new ways of propulsion are being explored for spacecraft. One such method is the use of a solar sail. Solar sailing [13] is a technique that relies on solar radiation to generate propulsion in space. A large, thin, reflective screen is used to accelerate the spacecraft without using any fuel. Though the resulting acceleration from this solar radiation pressure is small, its continuous presence over longer time scales assures a gradual increase of velocity that can match and exceed conventional means of propulsion. In doing so, solar sails have the potential to be a sustainable technique for long duration missions. Because they use sunlight as their power source, there is a minimal impact on the environment and the energy source is sustainable and inexhaustible. This means that as long as the sail remains functional and the spacecraft's communication and other systems remain operational, a solar sail spacecraft can potentially operate indefinitely. This makes them an outstanding propulsion method for long-duration missions that may require a continuous line of support.

Although the idea of solar sailing was already popularized in the 1970s, when Carl Sagan proposed a rendezvous mission to Halley's comet (which unfortunately never came to fruition), it was only relatively recently when the first solar sail mission saw the light of day. In 2010, JAXA launched the world's first solar sail spacecraft, fittingly dubbed 'IKAROS' [15]. Sporting a 14 by 14 m sail made of 7.5μm polyimide (about 1/10th of a human hair), it succesfully utilized solar radiation pressure to accelerate and control its orbit. Later that year, NASA launched the Nanosail-D2, a smaller solar sail with a sail area of around 10m^2, to test sail deployment techniques and gather other solar sail specific operational data [11]. The Planetary Society followed up suit with the LightSail 1 and LightSail 2 spacecraft, two crowdfunded technology demonstration missions [21]. All these missions have showcased the immense potential of solar sails.

1.1.2. Cyclers

As industry is finding its place in space, future missions will see increasing operation lifetimes. For long duration missions such as asteroid resource utilization (e.g., mining of rare-Earth metals and minerals), sustainable logistics are an important aspect of mission design. Cyclers pose a very interesting set up for these operations and the application of a solar sail can increase sustainability significantly. A cycler is a spacecraft that repeatedly visits two (or more) bodies in a cyclic pattern. To set up a cycler spacecraft, the end conditions of one cycle must be the same as the initial conditions. In other words, the position of the celestial bodies and the spacecraft in question are in the same relative or absolute position with respect to a certain reference frame. This requires careful consideration of the cycle time and an optimization of the outbound and inbound transfer trajectories with respect to their time of flight.

In 1969, ballistic cycler trajectories were found for an Earth-Venus cycler [10]. In 1985, Buzz Aldrin followed with similar ballistic trajectories for an Earth-Mars cycler [1]. These showed the potential of cyclic trajectories using conventional propulsion methods. The spacecraft would require initial insertion into the cycler orbit but no further propulsion afterwards, apart from guidance corrections for possible perturbations.

Earlier work on solar sail cyclers has been done for an Earth-Mars cycler in Reference [23]. In that work, the Circular Restricted Three-Body Problem (CR3BP) is used to approximate the dynamics of the spacecraft in the vicinity of a planet. This model gives rise to gravitational equilibrium points in a Sun-planet system, the so-called Lagrange points. In theory, a spacecraft could remain at rest at a Lagrange point if undisturbed. In practice, spacecraft will be in a periodic orbit around a Lagrange point. These Lagrange points in turn give rise to invariant manifolds, trajectories along which a spacecraft will naturally move when given a small perturbation or along which the spacecraft could naturally glide towards the Lagrange point. The use of invariant manifolds proves useful for finding heteroclinic-like connections between the Sun-Earth Lagrange point 2 and the Sun-Mars Lagrange point 1. The cycle time is then minimised using the synodic period of Mars with respect to Earth (or, conversely, the dwelling times at these points is maximized). The synodic period is the time between consecutive relative configurations of two celestial bodies (i.e., they have the same angle between them in a certain reference frame). The cycle time is chosen as the smallest integer multiple of the synodic period that fits the minimised time of flight. The time optimal trajectories found in that work showcased the feasibility of setting up a solar sail cycler between Lagrange points of different Sun-planet systems.

1.1.3. Near-Earth Asteroids

This thesis aims to expand upon this solar sail Earth-Mars cycler by investigating the possibility of connecting a Sun-Earth Lagrange point to a Sun-asteroid Lagrange point. Asteroids are rocky objects in space that orbit the Sun, similar to planets but much smaller. Several missions have targeted asteroids over the past, including (but not limited to) NASA's NEAR Shoemaker [18], JAXA's Hayabusa and Hayabusa2 (which managed to return a sample of 5 grams to Earth [12]) and NASA's OSIRIS-REx (which managed to collect a sample of between 400 grams and over 1 kg [9]). Whereas these missions managed to collect small amounts of samples, it is not unlikely for future mining operations to take place at asteroids, requiring continuous logistical support for transport of materials.

There are many asteroids in the Solar System, and most are categorized in three major groups: Jupiter's Trojan asteroids, the Main Belt Asteroids (MBAs) and the Near-Earth Asteroids (NEAs). While the methods described in this work could be utilized for cyclers between Earth and any asteroid in the Solar System, this work focuses on Near-Earth Asteroids (NEAs). NEAs should not be confused with Near-Earth Objects (NEOs) as that grouping also contains comets. Comets are excluded from this study because their composition contains less metallic and more icy materials. Though icy materials offer other benefits (such as in situ fuel generation), this work targets asteroids because their metallic composition is of high value [2].

Because asteroids are much smaller than planets, they give rise to a significantly different dynamical environment than a planetary environment. They therefore require different dynamical models to approximate the dynamics of a spacecraft in their vicinity. The Hill problem [22] is a more suitable model for these kinds of bodies. The necessity for different dynamics is even more apparent when the asteroid is in a highly eccentric orbit. The power of incoming solar radiation and the gravitational attraction of the Sun decrease with distance from the Sun, so a highly eccentric asteroid orbit will give rise to a non-constant force resulting from the solar sail. This time-dependency turns the problem into a non-autonomous problem, increasing the complexity of the system. The Elliptic Hill (Three-Body) Problem (EH3BP) [19, 20, 6] is therefore investigated for this particular application.

1.2. Research Objective and Questions

As a first step towards investigating solar sail asteroid cyclers, the methodology has to be investigated. This thesis focuses on investigating a cycler setup with the EH3BP to an 'easy' target to showcase the feasibility of solar sail Earth-asteroid cyclers. Therefore, finding a suitable target is the first objective of the thesis. The Sun-Earth CR3BP is connected to the EH3BP with an intermediate phase using a two-body problem. After showing this set up of the dynamical models works for the target asteroid, it can be tested on more difficult targets. Furthermore, the use of the synodic period is investigated for a solar sail asteroid cycler.

This leads to the following research objective for this thesis:

> **CAN A HETEROCLINIC-LIKE CONNECTION BE FOUND BETWEEN THE $\mathrm{SE}-\mathrm{L2}$ POINT AND THE $\mathrm{Sa}-\mathrm{L1}$ POINT OF A SUITABLE ASTEROID TO DEMONSTRATE THE FEASIBILITY OF SETTING UP A SOLAR SAIL EARTH-ASTEROID CYCLER?**

In an effort to reach the research objective, the following research questions have been framed:

1. **What physical characteristics are of consideration when selecting the initial target asteroid and which orbital characteristics distinguish an easy to reach target from a more difficult to reach target?**
2. **What is the minimum time-of-flight of the transfer trajectories between $\mathrm{SE}-\mathrm{L2}$ and $\mathrm{Sa}-\mathrm{L1}$ and what are therefore the maximum dwelling times at these points for the solar sail asteroid cycler to the asteroid selected through Research Question Q-1?**
3. **What is the quality of the heteroclinic-like connections found between $\mathrm{SE}-\mathrm{L2}$ and $\mathrm{Sa}-\mathrm{L1}$ of the target asteroid that was selected in Research Question Q-1?**

1.3. Report Outline

This thesis report is written in the form of a journal article, formatted to the American Institute of Aeronautics and Astronautics (AIAA) template[1]. The article can be found in Chapter 2. It gives a short introduction to the problem after which the problem definition is given. Subsequently, the required dynamical models are described mathematically. This is followed by the optimal control problem and optimization techniques used; the initial guess generation techniques and sub-optimal results; and the final optimized results. The article concludes with a conclusion on the results and work.

After the journal article, the verification and validation of the work is given in Chapter 3. Finally, an overarching conclusion is given in Chapter 4 with regards to the thesis research objective and research questions along with recommendations for future research.

[1]https://www.aiaa.org/publications/journals/Journal-Author

2
Journal Article

Time optimal heteroclinic-like connections for a solar sail Earth-asteroid cycler between Sun-Earth L_2 and Sun-asteroid L_1 of asteroid 2001AE2

Olivier M. van Bon
Delft University of Technology, 2629 HS Delft, The Netherlands

This work investigates the possibility of setting up an Earth-asteroid cycler to asteroid 2001AE2 using solar sail technology. An ideal solar sail model with near-future technology levels ($\beta = 0.05$) is implemented alongside the circular restricted three-body problem, two-body problem and the elliptic Hill problem. The spacecraft cycles between the Sun-Earth L_2 point ($\mathrm{SE-L2}$) and the Sun-asteroid L_1 point ($\mathrm{Sa-L1}$). From these equilibrium points, the spacecraft state vector is propagated forwards and backwards with a constant sail attitude to generate solar-sail assisted invariant manifolds. Initial guess trajectories for the outbound and inbound sections of the cycle are generated with a genetic algorithm by searching for optimal sail attitudes for the different dynamical models and departure, connection and arrival times. These initial guess trajectoryies are used to seed the optimization software PSOPT. This pseudospectral collocation method using Legendre-Chebyshev polynomials transforms the infinite dimensional control problem into a finite dimensional non-linear programming problem. This way a continuous control profile can be found that justifies the dynamical models and results in a time-optimal trajectory. The resulting cycler is designed to have a cycle time of 11.04 years, with an outbound trajectory departing from $\mathrm{SE-L2}$ on $01-03-2036$ and arriving at $\mathrm{Sa-L1}$ on $02-04-2039$ and an inbound trajectory departing from $\mathrm{Sa-L1}$ on $04-08-2043$ and arriving back at $\mathrm{SE-L2}$ on $31-03-2046$. This results in dwelling times at $\mathrm{SE-L2}$ of 351 days (0.95y) and at $\mathrm{Sa-L1}$ of 1585 days (4.34y). The trajectories are assumed time-optimal given the assumptions made in the work, but require further refining for non-ideal properties of the solar sail and other higher fidelity models.

I. Introduction

Solar sailing is an innovative propulsion technique that has slowly gained attention over the past decades, through missions such as IKAROS [1] and the LightSail missions [2]. Whereas conventional methods of providing propulsion rely on propellant, a solar sail uses a thin, highly reflective screen to gain momentum from incident solar radiation [3]. The lack of propellant and limitless source of incident radiation result in a theoretically unlimited ΔV, making solar sails highly suitable for long lifetime missions. Only limited by the degradation of the sail material, they pose a sustainable means of spaceflight for long duration applications.

Solar sails have seen a lot of technological advancement over the past decade. A useful metric for the sail's performance is the lightness number β, defined as the ratio of the solar radiation pressure acceleration to the solar gravitational acceleration [3]. This dimensionless parameter is purely dependent on the sail mass-to-area ratio σ. Previous missions had a lightness number up to $\beta \approx 0.01$ (LightSail-1,2 [2] and NEAScout [4]) and near future missions are expected to reach lightness numbers up to $\beta = 0.05$ [5, 6], so that value is used in this work.

This work uses an ideal solar sail model as described by [3]. This decreases the complexity of the sail model, but does not greatly increase the time of flight. Based on the results of [7], an increase of $\sim 10\%$ can be expected for the time of flight when using more realistic models.

Various other sail models exist to account for non-ideal properties of the sail [3]. Optical sail models account for non-perfect reflectivity due to absorption and re-radiation and a parametric force model can be used to account for billowing of the sail. As this work is intended to serve as a preliminary study into Earth-asteroid cyclers, these models will not be used and instead an ideal sail model is employed. In this work, perfect reflectivity is assumed in combination with a flat sail.

A. Cyclers

Through cyclic patterns and orbital resonances of different celestial bodies orbiting the Sun, a so-called *cycler* can be set up. A cycler can provide a continuous line of transportation between two (or more) bodies with minimal to no need for adjusting its transfer trajectories.

Earlier work on cyclers include the ballistic cycler trajectories found between Earth and Venus by [8], and between Earth and Mars - also known as the Aldrin cycler [9]. These use conventional propulsion methods and therefore are no

This work investigates the use of solar sails to set up a cycler between Earth and asteroids by searching for a repeatable set of trajectories that connect the Sun-Earth L_2 libration point with a Sun-asteroid L_1 point and vice versa. Solar sail transfers between libration points of different Sun-planet systems have already been investigated [10], which Reference [11] extended by setting up an Earth-Mars cycler. This work sets out to extend this further, towards an Earth-asteroid cycler. The methodology aims to be applicable to any asteroid, but a single target asteroid is used to verify the techniques used.

B. Near-Earth Asteroids

Aside from the scientific interest in asteroids, future long term interests include the utilization of material resources [12]. This work is intended to be a stepping stone towards the logistics of these kinds of operations, not just limited to the utilization of materials but also to, for example, provide support for long term crewed operations.

From a scientific point of view, there is great interest in asteroid missions because they are remnants of the early Solar System and contain valuable information about the evolution of the Solar System [13].

There are many asteroids in the Solar System, and most are categorized in three major groups: Jupiter's Trojan asteroids; the Main Belt Asteroids (MBAs) and the Near-Earth Asteroids (NEAs). While the methods described in this work could be utilized for cyclers between Earth and any asteroid in the Solar System, this work focuses on Near-Earth Asteroids (NEAs). NEAs should not be confused with Near-Earth Objects (NEOs) as that grouping also contains comets. Comets are excluded from this study because their composition contains less metallic and more icy materials. Though icy materials offer other benefits (such as in situ fuel generation), this work targets asteroids because their metallic composition is of high value [12].

The size distribution of known NEAs and their estimated group sizes are detailed in Table 1. For each size range, the number of known asteroids and estimated group size are listed. The total number of NEAs is estimated to be approximately $(4 \pm 1) \times 10^8$, though only a small fraction of these are of size larger than 40m. While these relatively large asteroids make up ±70% of the observed population, they constitute only 0.13% of the total estimated NEA population. Evidently, it is more difficult to observe smaller asteroids (e.g., up to 40m).

Asteroid size	Number of known asteroids (% of total)	Estimated group size (% known)
$D > 1$km	889 (3.6%)	~ 920 (97%)
1km $> D >$ 140m	8,593 (34.8%)	~ 25,000 (34%)
140m $> D >$ 40m	7,556 (30.6%)	~ 500,000 (1.5%)
40m $> D >$ 20m	4,243 (17.2%)	~ 2,500,000 (0.17%)
20m $> D$	3,400 (13.8%	$\sim 4 \pm 1 \times 10^8$ (0.006%)
Total	24,668 (100%)	$\sim 4 \pm 1 \times 10^8$ (0.006%)

Table 1 Size distribution of known NEAs [14] and estimated group sizes [15].

Apart from size, there are two other classifications for NEAs which are relevant to this work: their orbital classification and spectral classification. The orbital classification defines four classes based on their perihelion and aphelion distance: the Apollo, Amor, Aten and Atira classes. This work aims to be applicable to any NEA, regardless of orbital classification. See Section II.B for more on the target selection procedure.

The spectral classification is taken into minor consideration though, as it can give an indication of (surface) composition. This can either increase capital profitability (for resource utilization) or scientific interest based on the spectral type. Two important spectral classifications are the Tholen class [16] and the SMASSII class [17].

The Tholen classification divides asteroids in three groups: carbonaceous (C-group), silicaceous (S-group) and an umbrella group (X-group) containing (among others) the "metallic" M-type asteroids. The more recent SMASSII classification is based on the Tholen classification and uses groups similar to the ones used by Tholen, but includes many sub-types.

Table 2 Summary of asteroid taxonomic classes [18].

Tholen Class	SMASS/Bus Class	Albedo
A	A	Moderate
B, C, F, G	B, C, C_b, C_h, C_g, C_{hg}	Low
D	D	Low
E, M, P	X, X_c, X_e, X_k	From low (P) to very high (E)
Q	Q	Moderate
R	R	Moderate
S	S, S_a, S_k, S_l, S_q, S_r	Moderate
T	T	Low
V	V	Moderate
-	K	Moderate
-	L, L_d	Moderate
-	O	-

An overview of the albedo of the different classes and types of asteroids identified by the Tholen and SMASS/Bus classifications are listed in Table 2 [18]. The albedo p_V (in the visual band) can be used in combination with the absolute magnitude H to determine the size of an asteroid (in [km]) [19], through

$$D = \frac{1329}{\sqrt{p_V}} 10^{-H/5} \tag{1}$$

II. Problem Definition

In this work, solar-sail transfer trajectories are investigated and optimized for an Earth-asteroid cycler. Section II.A will describe how the solar-sail cycler is set up. From all NEAs described in Section I.B, a target asteroid will be selected that this work will focus on. The selection process is described in Section II.B

A. Cyclers and Synodic Periods

As described in Section I.A, a cycler is a spacecraft that originates from a specified place (be it a specific orbit or a specific point in space), travels to one or more places and returns to its origin, creating a cyclic pattern of transfer trajectories. The repeated part of a cycler is called a cycle. In this work, a cycle is investigated and optimized from the vicinity of Earth to the vicinity of an asteroid.

This cycle can be described by an outbound trajectory (Earth to asteroid) and an inbound trajectory (asteroid to Earth), each subdivided into several phases. Section III will elaborate on the dynamical models used for these phases. From these dynamics originate so-called libration points in the Sun-Earth and Sun-asteroid synodic frames. The departure point is set at the Sun-Earth Lagrange point 2 (SE – L2) and the arrival point is set at the Sun-asteroid

Lagrange point 1 (Sa – L1).

Earlier work on solar-sail cyclers has been done by [11]. In that work, a cycler was set up between Earth and Mars, both in nearly circular, coplanar orbits around the Sun. This allows the cycler pattern to make use of the synodic period of the two bodies.

The synodic period T_{syn} is the time between conjunctions of two bodies orbiting a third body or, alternatively, the time between two consecutive configurations where the angle ϕ between the two bodies in an inertial reference frame is the same, given by

$$\frac{1}{T_{syn}} = \frac{1}{T_1} - \frac{1}{T_2} \tag{2}$$

where T_1 and T_2 are the orbital periods of the two orbiting bodies. This is illustrated in Figure 1 (a).

The synodic period is illustrated schematically in Figure 1. Two consecutive configurations with the same relative position are shown for a target body with a) a circular coplanar orbit, b) an eccentric orbit, and c) an inclined orbit with respect to Earth's orbit. If the target asteroid has an eccentric or inclined orbit, it is no longer possible to use the synodic period. When Earth and the asteroid are in the same relative angular configuration, the asteroid can be at a very different segment in its orbit (i.e., true anomaly) for an asteroid in a non-circular, non-coplanar orbit, as illustrated in Figure 1 b) and c).

Using Equation 2, the synodic period of Earth ($T = 1yr$) and Mars ($T = 1.881yr$) is found to be $T_{syn} = 2.135yr$. This means that every 2.135 years, Mars can be found in the same relative position in its orbit with respect to Earth. Using this relationship, a cycle can be set up with a cycle period T_{cyc} of any integer multiple of T_{syn}, i.e. $T_{cyc} = n_T T_{syn}$. However, when transferring to an eccentric or inclined orbit, this is not as straightforward.

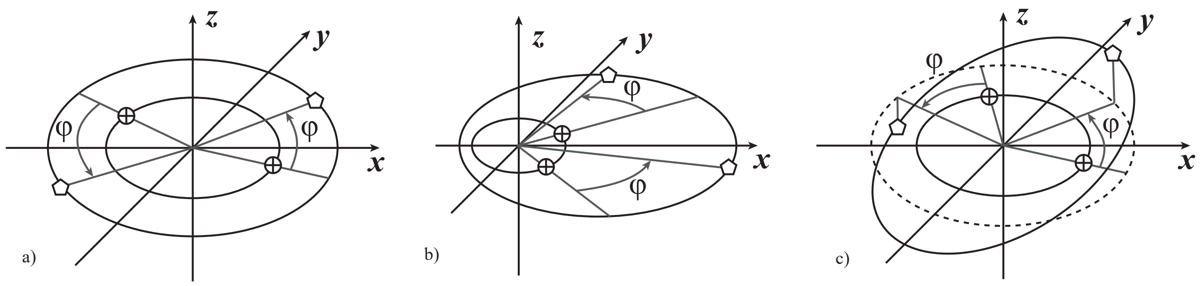

Fig. 1 Consecutive configurations where the angle between Earth (⊕) and the target asteroid (⬠) is the same in an inertial reference frame for a) a circular coplanar asteroid orbit, b) an elliptical coplanar asteroid orbit and c) an inclined asteroid orbit.

In order to configure a set of repeatable trajectories, both Earth and the asteroid must return as close to their initial true anomaly at the end of a cycle as possible. In other words, the bodies need to return to the same absolute position with respect to each other, instead of the same relative position. A straightforward way to do this would be to require the asteroid's orbit to exhibit a mean-motion resonance (MMR) with respect to Earth's orbit,

$$n_{ast} : n_{Earth} = k_1 : k_2 \tag{3}$$

where n is the body's mean motion and k_1, k_2 are small integers.

This relation indicates that the asteroid completes k_1 orbits in the time that Earth completes k_2 orbits. The cycler period can then be taken to be $T_{cyc} = k_2$ years. An upper limit for k_2 is set to limit the search space and limit the cycler time. To generalize this, the maximum value for k_2 is based on the time it takes to reach an orbit with a high inclination, as large plane changes generally take the most time of orbital maneuvers. The maximum inclination change per revolution around the Sun for a (non-ideal) solar sail with $\beta = 0.05$ was shown to be 4deg by [20], indicating that to reach an orbit with an inclination as high as 30deg a minimum of 7.5 revolutions are required. A very crude translation of this into a transfer time of 7.5 years means a cycle will already require 15 years. In that case, the search space for the MMR should be limited to around $k_2 \leq 15$. For a coplanar target orbit, this can be even smaller since the transfer trajectory does not need many revolutions to accommodate the plane change.

Though this process is straightforward, it is nonetheless difficult. Asteroids do not generally exhibit a perfect MMR pattern with Earth. To accommodate for the delay or advancement of Earth at the end of the cycle and allowing the asteroid to return to its initial position, the MMR mismatch ϵ_{cyc} is defined, given by

$$n_{ast} : n_{Earth} = k_1 : (k_2 + \epsilon_{cyc}) \tag{4a}$$

$$\epsilon_{cyc} = k_1 \frac{n_{Earth}}{n_{ast}} - k_2 = k_1 \frac{T_{ast}}{T_{Earth}} - k_2 \tag{4b}$$

In other words, the asteroid is allowed to run its full cycle with Earth misplaced slightly at the end of the cycle, expressed as a fraction of its orbit ϵ_{cyc}. This parameter is one of the criteria used in the asteroid selection process described in Section II.B.

Although ideally a cycler is designed to remain operable indefinitely, it is important to consider how long an imperfect cycle can be used before the cycle trajectory needs to be modified. To illustrate the limits of the MMR mismatch, the MMR mismatch is calculated for Mars, which is often assumed to be circular. For a maximum cycle time of $T_{cyc} = 10$y (i.e., $k_2 \leq 10$), the MMR mismatch is $\epsilon_{cyc} = 0.119$ with an MMR of $k_1 : k_2 = 1 : 2$. Only when increasing the cycle time to $T_{cyc} = 15$y ($k_2 = 15$) does the MMR mismatch decrease to $\epsilon_{cyc} = 0.0468$ with an MMR of $k_1 : k_2 = 8 : 15$. In this work, the orbit of Mars is used as an upper limit for the MMR mismatch to validate its use for asteroids.

B. Target Selection

This work should ideally be applicable to any NEA. However, limitations have been applied as this is a first step towards solar-sail asteroid cyclers. A few filters have been chosen to select a target asteroid from the large population of NEAs described in Section I.B. These filters are shown schematically in Figure 2. The filters are purposefully chosen in a restricting way in order to test the dynamical models and cycler design. The resulting asteroid is preferably in an orbit that is near-circular and has a very small inclination. This is done to ensure that if there is no valid MMR mismatch available the use of the synodic period is still justified. Future work is necessary to loosen these filters and verify that the methods also work on asteroids with less restricted orbits in terms of eccentricity and inclination. The rest of the methodology is set up assuming the MMR is used and so it should be applicable to all asteroids, regardless of eccentricity or inclination.

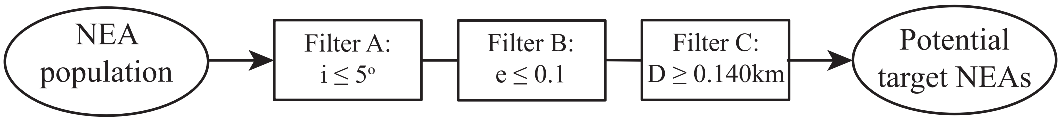

Fig. 2 Selection filters used in the target asteroid selection.

First, an inclination filter is used. This decreases the amount of revolutions required to accommodate for the plane change, which keeps the transfer time smaller. This filter was chosen based on the maximum inclination change (Δi = 4deg after 1 revolution around the Sun) for a solar sail (with $\beta = 0.05$) cranking orbit purely dedicated to changing the inclination [20]. The trajectory optimization technique in this work does not separate the transfer orbit into separate parts for changing the semi-major axis, eccentricity and inclination, but rather performs all of these changes smoothly over the course of the trajectory. Therefore, the maximum inclination is chosen to be limited to $i \leq 5°$, which allows for the assumption of the orbit being coplanar to be made.

Secondly, an eccentricity filter is used to only select asteroids with a nearly circular orbit. The maximum allowed eccentricity chosen is approximately that of Mars' orbit. Mars has one of the highest orbital eccentricities of all planets, second only to that of Mercury. In other studies, Mars' orbit is often assumed to be circular. This allows the use of the synodic period and increases the ease of finding a suitable target asteroid. Hence, in this work the maximum eccentricity is set to $e \leq 0.1$.

The combination of filter A and B will allow the use of the synodic period if there is no asteroid with a small enough MMR mismatch. At that point, the asteroid orbit will both be nearly circular and nearly coplanar with Earth's orbit - the two prerequisites for using the synodic period.

The third filter ensures that the target asteroid has a sizable diameter. This filter is chosen to increase the expected amount of materials to be extracted (one of the key points of interest for the asteroid cycler), as well as from an operational perspective. Small objects (below 150 – 200m) are often found to have high spin periods (down to the order of minutes) and can be in non-principal axis rotation states [21]. This can increase operational difficulty for complex surface operations which fly-by missions do not necessarily need to take into account. The value for the filter is based on the asteroid size distribution shown in Table 1. A diameter of $D \geq 0.140$km keeps a large part of the population, but disposes of the many small ones that are less likely to contain large quantities of interesting materials. For asteroids with missing data, their diameter is estimated from other available data, such as their absolute magnitude H, spectroscopic class and albedo p_V.

Finally, the population is sorted based on ϵ_{cyc}. The MMR mismatch is not set as a filter as this work is not about a specific mission design and this would require further assumptions on mission lifetime and cycle time. But the MMR mismatch is still used as a ranking, to ensure the target asteroid has an orbital period that can be related to a cycle time with only a small error between the final and initial conditions.

The resulting list of asteroids is shown in Table 3. Asteroid data are taken from [22], with the diameter estimated from other available data. The number of possible target asteroids in the list is very small, due to the restrictive filters used. This is is deemed justified by noting once more that this work is intended as an initial proof of concept for solar sail Earth-asteroid cyclers.

Table 3 List of potential target asteroids resulting from the filters in Figure 2 and Mars for reference. Best mean motion resonance parameters $k_{1,2}$ and mismatch ϵ_{cyc} listed for maximum cycler times of $T_{cyc} \leq 15$y and $T_{cyc} \leq 8$y. Asteroid data for i, e and T_{ast} taken from [22]. Mars data taken from [23].

Object	e	i[deg]	D_{est}[km]	T[y]	T_{syn}[y]	$\epsilon_{cyc}[-]$ $T_{cyc} \leq 15$	k_1	k_2	$\epsilon_{cyc}[-]$ $T_{cyc} \leq 8$	k_1	k_2
2001 AE2	0.0815	1.66	0.452	1.567	2.760	0.0245	7	11	0.135831	2	3
2001 SW169	0.0515	3.55	0.462	1.394	3.533	0.0262	5	7	0.026229	5	7
1996 XB27	0.0579	2.46	0.146	1.296	4.375	0.0371	10	13	0.11114	3	4
Mars	0.0934	1.85	3396.2	1.881	2.135	0.0468	8	15	0.11915	1	2

The MMR mismatch of Mars for $T_{cyc} = 15$y is $\epsilon_{cyc} = 0.0468$, which translates to a delay of Earth's position in its orbit at the end of the cycle of ~ 17 days. For all three asteroids the MMR mismatch for a maximum cycler time of $T_{cyc} \leq 8$y is similar to that of Mars. When the maximum cycler time is increased to $T_{cyc} \leq 15$y, the MMR mismatch ϵ_{cyc} is smaller than that of Mars for all asteroids listed. Combined with the effect of the inclination and eccentricity filters, the use of the synodic period from Equation 2 is deemed justified for all there asteroids.

The asteroid with the lowest value for ϵ_{cyc} (asteroid 2001 AE2) also has the lowest inclination, an average eccentricity and a large diameter, relative to the rest of the filtered population. It is the only one of the three asteroids, for which both the eccentricity and inclination are smaller than that of Mars. Additionally, it is the only one in this list whose spectral type has been measured. It is a SMASSII T-type asteroid [21], possibly indicating a "primitive" composition. For initial asteroid cyclers these types of asteroids can be especially interesting from a scientific perspective, as their primitive composition can be tied to the early Solar System. The D and T classes are of special interest, though they are mostly found in the outer asteroid belt and among Jupiter Trojans [21]. It is therefore chosen as the target asteroid for this study.

The orbit of 2001AE2 has a semi-major axis of $a_{ast} = 1.349614268$AU and is shown in Figure 3[22]. With an orbital period of $T_{ast} = 1.567916$y, the resulting near-perfect MMR is $n_{ast} : n_{Earth} = 7 : (11 - 0.02459)$, i.e., the asteroid completes 7 revolutions in a cycle and Earth completes almost 11 revolutions. Every cycle Earth accumulates a delay of 0.02459×365d $\approx$ 9d. Since this would mean that the orbit would have to be changed after two cycles (according to the illustrative example above), the MMR-mismatch method is not applied and the synodic period ($T_{syn} = 2.760$y) is used instead with the assumption that the orbit is both nearly circular and nearly coplanar. Then, the cycle time is set as a multiple of the synodic period.

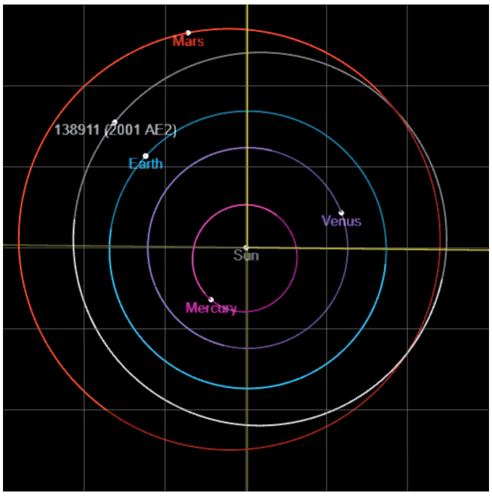

Fig. 3 Orbit of asteroid 2001AE2 [22].

III. Dynamical Models

In this section the dynamical models are described that are used to find the solar-sail trajectories. Section III.A gives a qualitative description of the three different dynamical models. The subsequent subsections present a mathematical description of the models.

A. Required Dynamical models

The motion of the spacecraft is described in relation to the Sun, Earth and target asteroid (2001 AE2). Previous work on a solar sail cycler, investigated transfers between Earth and Mars [11]. In that scenario, the motion of the spacecraft can be well approximated by the Circular Restricted Three-Body Problem (CR3BP) [24]. This framework describes the motion of an infinitesimally small mass m under the influence of two larger bodies (often called the primaries) with masses m_1 and m_2. Secondly, it assumes the orbit of the two primaries around each other to be circular. Section III.B describes this model into more detail. The CR3BP works well to describe the motion of a spacecraft in the vicinity of both Earth and Mars, with the Sun acting as the second primary. Both Earth and Mars have a large mass compared to the spacecraft and their orbits around the Sun have a small eccentricity. To describe a transfer from the vicinity of Earth to the vicinity of Mars, the CR3BP of the Sun-Earth and Sun-Mars systems are patched together.

For the motion of a spacecraft in the vicinity of an asteroid, those two requirements are not always met. Firstly because asteroids have a relatively small mass compared to planets and secondly because their orbit is not necessarily circular. Therefore the motion in the vicinity of the asteroid is better described by the Elliptic Hill Three-Body Problem (EH3BP). This model works well when the mass of one of the two primaries is not very large and when the eccentricity of its orbit is not necessarily small. Section III.C describes this model in more detail. While the target asteroid 2001 AE2 does not have a high eccentricity, the model was still incorporated as it also works for circular orbits and with future work on elliptic asteroid orbits in mind.

Patching a circular to an eccentric trajectory can be difficult, so an intermediate phase is introduced using the simpler (Sun-Sail) Two-Body Problem (SS2BP). Section III.D describes this model in more detail.

The cycler is separated into different phases, each of which uses one of the three dynamical models. The complete outbound transfer from Sun-Earth L_2 ($SE - L2$) to Sun-asteroid L_1 ($Sa - L1$) is given by three phases:

1) Phase O_1: Departure trajectory from $SE - L2$, using the CR3BP.
2) Phase O_2: Intermediate trajectory, using the SS2BP.
3) Phase O_3: Arrival trajectory towards $Sa - L1$, using EH3BP.

The complete inbound transfer from Sun-asteroid L_1 ($Sa - L1$) to Sun-Earth L_2 ($SE - L2$) is subsequently given by:

1) Phase I_1: Departure trajectory from $Sa - L1$, using EH3BP.
2) Phase I_2: Intermediate trajectory, using the SS2BP.
3) Phase I_3: Arrival trajectory towards $SE - L2$, using the CR3BP.

These phases are shown schematically in Figure 4. In between the outbound and return phases are parking phases, in which the spacecraft is assumed stationary at the Lagrange point for simplicity. In reality, the CR3BP and EH3BP will have to be connected to libration point orbits, such as a halo orbit or Lyapunov orbit.

All three models are complimented by the solar sail acceleration, as described below.

B. Circular Restricted Three-Body Problem

The CR3BP describes the motion of an infinitesimally small mass m (the spacecraft) under gravitational influence of two larger masses m_1 (the Sun) and m_2 (Earth). The two larger bodies move around their center of mass in circular orbits and the gravitational influence of the small mass on the two primaries is assumed to be negligible [24].

The motion of the spacecraft is described in a synodic reference frame $C(\hat{\boldsymbol{x}}, \hat{\boldsymbol{y}}, \hat{\boldsymbol{z}})$, with its origin at the Sun-Earth barycenter, the $\hat{\boldsymbol{x}}$ axis pointing towards Earth, the $\hat{\boldsymbol{z}}$ axis pointing perpendicular to the Sun-Earth orbital plane, and the $\hat{\boldsymbol{y}}$ axis completing the right-handed frame, see Figure 5. The reference frame is rotating around the $\hat{\boldsymbol{z}}$ axis at a constant

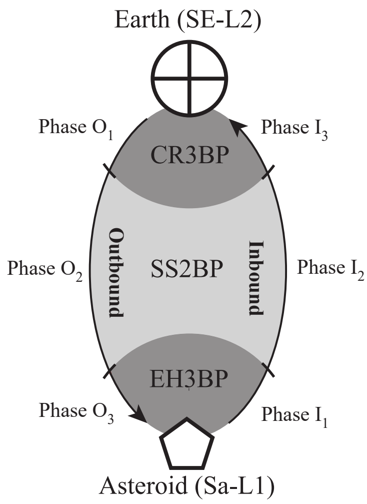

Fig. 4 Overview of the dynamical models used in the cycler trajectories.

angular rate $\hat{\omega} = \omega\hat{z}$. A new set of units is defined for mass, length and time, based on the primaries of the system. The unit of mass is $m_1 + m_2$, the unit of length λ is the distance between m_1 and m_2 and the unit of time is $\tau = 1/\omega$. The mass ratio $\mu_{CR} = m_2/(m_1 + m_2)$ is defined to further non-dimensionalize the system. The dimensionless mass of the Sun and Earth become $1 - \mu_{CR}$ and μ_{CR}, respectively. Their positions along the $\hat{\boldsymbol{x}}$ axis become $-\mu_{CR}$ and $1 - \mu_{CR}$, respectively. In the Sun-Earth CR3BP the mass, length and time scales are given by

$$\mu_{CR} = 3.003480 \times 10^{-6} \qquad \lambda_{CR} = 1.495978 \times 10^{8} \text{ km} \qquad \tau_{CR} = 5.022635 \times 10^{6} \text{ s} \tag{5}$$

.

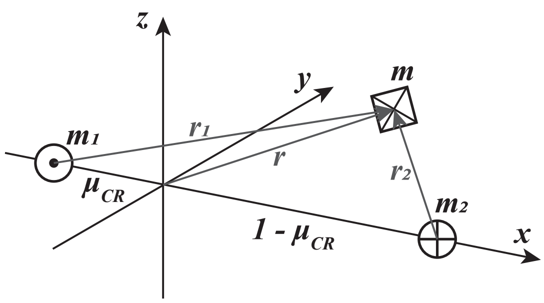

Fig. 5 Schematic view of a solar sail in the Sun-Earth CR3BP reference frame.

The equations of motion for a solar sail in the CR3BP are given by [3]

$$\ddot{\boldsymbol{r}} + 2\omega \times \dot{\boldsymbol{r}} + \nabla U = \boldsymbol{a}_s \tag{6}$$

The terms on the left-hand side of Equation 6 represent the general CR3BP, whereas the term on the right-hand side represents the acceleration $\boldsymbol{a}_s$ induced by the solar sail. The dimensionless position vector $\boldsymbol{r}$ of the spacecraft and its derivative (the velocity vector $\dot{\boldsymbol{r}}$) give the spacecraft state vector $\boldsymbol{s} = \begin{bmatrix} \boldsymbol{r} & \dot{\boldsymbol{r}} \end{bmatrix}^T$. The effective potential U is the combined potential of the three-body gravitational potential V and the potential Φ of the centripetal force, given by

$$U = V + \Phi = -\left(\frac{1-\mu_{CR}}{\mathrm{r}_1} + \frac{\mu_{CR}}{\mathrm{r}_2}\right) - \frac{1}{2}\left(x^2 + y^2\right) \tag{7}$$

where r_1 is the dimensionless distance from the Sun to the sailcraft and r_2 is the dimensionless distance from Earth to the sailcraft.

The solar-sail induced acceleration $\boldsymbol{a}_s$ is based on an ideal sail model, assuming a flat sail and perfect reflection of incident radiation [3]. In future work, an optical or parametric sail model could also be employed. These models take into account optical properties (e.g. absorption and re-radiation) and billowing of the sail, respectively, resulting in a more accurate representation of the force vector resulting from the solar radiation pressure.

In the ideal sail model, the solar sail acceleration vector acts aligned along the normal vector $\hat{\boldsymbol{n}}$ of the sail and is defined as [3]

$$\boldsymbol{a}_s = a_s \hat{\boldsymbol{n}} = \beta \frac{1-\mu_{CR}}{r_1^2} \left(\hat{\boldsymbol{r}}_1 \cdot \hat{\boldsymbol{n}}\right)^2 \hat{\boldsymbol{n}} \tag{8}$$

where dimensionless parameter β is the sail's lightness number. The term $\left(\hat{\boldsymbol{r}}_1 \cdot \hat{\boldsymbol{n}}\right)^2$ accounts for the reduced projected solar sail area when the sail normal is not oriented along the direction of the incident radiation.

The lightness number can be described by the sail area to spacecraft mass ratio σ and the critical sail loading parameter $\sigma^* = 1.53\ \mathrm{g/m^2}$

$$\beta = \frac{\sigma^*}{\sigma} \tag{9}$$

Based on lightness numbers of past missions (IKAROS: $\beta = 0.001$[1]; Lightsail-1: 0.011[25]; NEA Scout: 0.010 [4]) and estimates for near-term missions of $\beta = 0.04$ and long-term missions of $\beta = 0.1$ [26], a lightness number of $\beta = 0.05$ was chosen for this work.

The orientation of the solar sail in the CR3BP is described using the cone angle α and the clock angle δ, see Figure 6. With respect to the Sun-sail line $\hat{\boldsymbol{r}}_1$, the normal vector of the sail is expressed as

$$\hat{\boldsymbol{n}}\big|_{\hat{\boldsymbol{r}}_1} = \begin{bmatrix} \cos\alpha \\ \sin\alpha \sin\delta \\ \sin\alpha \cos\delta \end{bmatrix} \tag{10}$$

This can be transformed to the Sun-Earth CR3BP frame through

$$\hat{\boldsymbol{n}} = \mathbb{R}\hat{\boldsymbol{n}}|_{\hat{\boldsymbol{r}}_1} \tag{11a}$$

$$\mathbb{R} = \begin{bmatrix} \hat{\boldsymbol{r}}_1 & \hat{\boldsymbol{\theta}} & \hat{\boldsymbol{\phi}} \end{bmatrix} \tag{11b}$$

with $\hat{\boldsymbol{\theta}}$ and $\hat{\boldsymbol{\phi}}$ as defined in Figure 6.

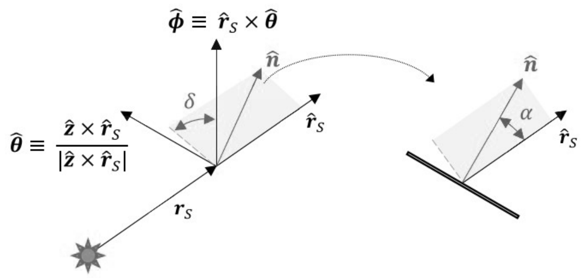

Fig. 6 Orientation of the solar sail within the Sun-Earth synodic frame [11].

C. Elliptic Hill Three-Body Problem

The EH3BP describes the motion of the sailcraft in vicinity of a smaller celestial body that is on a non-circular orbit. For this model, a rotating-pulsating reference frame $E(\hat{\boldsymbol{X}}, \hat{\boldsymbol{Y}}, \hat{\boldsymbol{Z}})$ is employed (see Figure 7), now with its origin at the asteroid, the $\hat{\boldsymbol{X}}$ axis pointing along the Sun-asteroid line, the $\hat{\boldsymbol{Z}}$ perpendicular to the asteroid's orbital plane and the $\hat{\boldsymbol{Y}}$ axis completing the right-handed reference frame. The frame rotates with a non-constant angular rate $\boldsymbol{\Omega} = \Omega\hat{\boldsymbol{Z}}$ around the $\hat{\boldsymbol{Z}}$ axis, due to the non-constant orbital velocity of the asteroid around the Sun. The Hill problem is valid as long as the distance of the spacecraft to the asteroid within the system is much smaller than the distance of the asteroid to the Sun $\boldsymbol{r}_1$, i.e. $\boldsymbol{R} \ll \boldsymbol{r}_1$[27]. The coordinates (X, Y, Z) are scaled in relation to the varying Sun-asteroid distance through the dimensionless parameter ρ

$$\rho = \frac{1}{1 + e\cos\nu} \tag{12}$$

where e is the eccentricity of the asteroid's orbit around the Sun and ν the asteroid's true anomaly [28].

The new effective potential is

$$U = \frac{\mu_{ast}}{R} - \frac{1}{2}\Omega^2\left(Z^2 - 3X^2\right) \tag{13}$$

where μ_{ast} is the gravitational parameter of the asteroid and R is the distance between the spacecraft and the center of the asteroid [29].

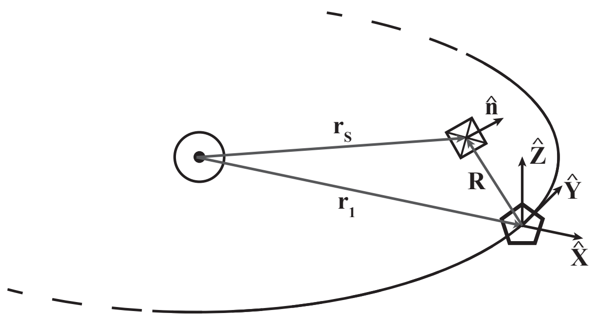

Fig. 7 Schematic of a solar sail in the rotating-pulsating reference frame $E(\hat{X}, \hat{Y}, \hat{Z})$.

Because the EH3BP is used only in vicinity of the asteroid and the $\hat{\boldsymbol{X}}$ axis points along the Sun-asteroid line $\hat{\boldsymbol{r}}_1$, the incident radiation at the solar sail is assumed to always be directed along the $\hat{\boldsymbol{X}}$ axis during this part of the trajectory, or $\hat{r}_S \approx \hat{r}_1 = \hat{X}$. The solar-sail induced acceleration vector in the EH3BP is then

$$\boldsymbol{a}_s = a_s \hat{\boldsymbol{n}} = \beta \frac{\mu_{Sun}}{r_1^2} \left(\frac{1}{\mu_{ast} \Omega^4} \right)^{1/3} (\hat{\boldsymbol{r}}_1 \cdot \hat{\boldsymbol{n}})^2 \, \hat{\boldsymbol{n}} \tag{14}$$

where r_1 is the Sun-asteroid distance, μ_{Sun} is the gravitational parameter of the Sun [28]. The orientation of the sail reduces to the same form as Equation 10 without need to transform it.

The resulting scalar equations of motion are [28]

$$\ddot{X} - 2\dot{Y} = \frac{1}{1 + e\cos\nu} \left[-\frac{X}{\mathrm{R}^3} + 3x + a_{s,X} \right] \tag{15a}$$

$$\ddot{Y} + 2\dot{X} = \frac{1}{1 + e\cos\nu} \left[-\frac{Y}{\mathrm{R}^3} + a_{s,Y} \right] \tag{15b}$$

$$\ddot{Z} + Z = \frac{1}{1 + e\cos\nu} \left[-\frac{Z}{\mathrm{R}^3} + a_{s,Z} \right] \tag{15c}$$

The length and time scale of the EH3BP are given by

$$\lambda_{EH} = \frac{\mu_{ast}}{\mu_{Sun}}^{(1/3)} a_{ast} = 80.53\text{km} \qquad \tau_{EH} = \frac{1}{n_{ast}} = 7.874236 \times 10^6 s \tag{16}$$

with a_{ast} the semi-major axis of the asteroid and n_{ast} is the mean motion of the asteroid.

D. Sun-Sail Two-Body Problem

The departure and arrival phases are connected with an intermediate phase, for which the SS2BP is employed. This model uses two-body dynamics for the Sun-sail system with the addition of the solar-sail induced acceleration. In this model, an inertial heliocentric frame $H(\tilde{\boldsymbol{x}}_I, \tilde{\boldsymbol{y}}_I, \tilde{\boldsymbol{z}}_I)$ is used, with its origin at the Sun, the $\tilde{\boldsymbol{x}}_I$ axis pointing towards the vernal equinox, the $\tilde{z}_I$ axis oriented perpendicular to the ecliptic, and the $\tilde{\boldsymbol{y}}_I$ axis completing the right-handed reference frame. The tilde notation $\tilde{(\cdot)}$ is used here to denote a parameter dimensional units. The two body dynamics are then formulated as [30]

$$\frac{d^2\tilde{\boldsymbol{r}}_I}{d\tilde{t}^2} = -\frac{\tilde{\mu}_{Sun}}{\tilde{r}_I^2}\hat{\tilde{\boldsymbol{r}}}_I + \tilde{\boldsymbol{a}}_s \tag{17}$$

with $\tilde{\boldsymbol{r}}_I$ the position of the spacecraft and $\tilde{\mu}_{Sun}$ again the Sun's gravitational parameter. The solar-sail induced acceleration $\tilde{\boldsymbol{a}}_s$ is given by

$$\tilde{\boldsymbol{a}}_s = \beta\frac{\tilde{\mu}_{Sun}}{\tilde{r}_I^2}\left(\hat{\tilde{\boldsymbol{r}}}_I \cdot \hat{\boldsymbol{n}}\right)^2 \hat{\boldsymbol{n}} \tag{18}$$

with $\hat{\boldsymbol{n}}$ defined the same way as in the CR3BP (see Equation 10 and Equation 11).

E. Reference Frame Transformations

The trajectory phases described in Section III.A are linked in the optimization scheme, which requires the states at the linkage time to be transformed from one reference frame to the next. Linking between the CR3BP and SS2BP requires a transformation from the Sun-Earth synodic frame to the inertial heliocentric frame. Linking between the EH3BP and the SS2BP requires a transformation from the Sun-asteroid synodic frame to the inertial heliocentric frame.

1. CR3BP frame to inertial heliocentric frame

The transformation from frame $C(\hat{\boldsymbol{x}}, \hat{\boldsymbol{y}}, \hat{z})$ to frame $H(\tilde{\boldsymbol{x}}_I, \tilde{\boldsymbol{y}}_I, \tilde{z}_I)$, is done through the following steps. Note that $(\tilde{\cdot})$ is used to denote a parameter in dimensional units. To transform the CR3BP state vector $s = [\boldsymbol{r} \quad \dot{\boldsymbol{r}}]^T$ to the SS2BP state vector $\tilde{\boldsymbol{s}}_I = \left[\tilde{\boldsymbol{r}}_I \quad \dot{\tilde{\boldsymbol{r}}}_I\right]^T$, first the origin of frame R is translated to the the Sun,

$$\boldsymbol{r}' = \boldsymbol{r} + [\mu_{CR} \quad 0 \quad 0]^T\,, \tag{19}$$

Then, the CR3BP state vector is dimensionalized using λ_{CR} and τ_{CR} (as defined in Section III.B)

$$\tilde{\boldsymbol{r}}' = \lambda_{CR}\boldsymbol{r}', \qquad \dot{\tilde{\boldsymbol{r}}} = \frac{\lambda_{CR}}{\tau_{CR}}\dot{\boldsymbol{r}} \tag{20}$$

and the SS2BP state vector is found by

$$\tilde{\boldsymbol{r}}_I = \mathbb{T}(\phi)\tilde{\boldsymbol{r}}' \tag{21a}$$

$$\dot{\tilde{\boldsymbol{r}}}_I = \mathbb{T}_z(\phi)(\dot{\tilde{\boldsymbol{r}}} + \omega \times \tilde{\boldsymbol{r}}') \tag{21b}$$

where $\mathbb{T}_z$ is the rotation matrix around the z axis and ϕ the angle between the Sun-Earth line and vernal equinox.

Transforming the dimensionless time t_{CR} of the CR3BP to the dimensional time $\tilde{t}$ of the SS2BP is done by

$$\tilde{t} = (t_{CR} - \phi_0 \frac{\pi}{180.0})/(\frac{2\pi}{365.2563}) + t_0 \tag{22}$$

where $\phi_0 = 100.377°$ is the angle between the Sun-Earth line and vernal equinox at t_0 (1-1-2000 12:00).

2. EH3BP frame to inertial heliocentric frame

The reference frame transformation from the EH3BP to the inertial heliocentric frame of the SS2BP is given by the following steps. Here, the frame is first dimensionalized using λ_{EH} and τ_{EH}

$$\tilde{\boldsymbol{R}} = \lambda_{EH} \boldsymbol{R} \qquad \dot{\tilde{\boldsymbol{R}}} = \frac{\lambda_{EH}}{\tau_{EH}} \dot{\boldsymbol{R}} \tag{23}$$

Then, the origin of frame E is translated to the Sun. The Sun-asteroid distance is

$$\tilde{\boldsymbol{r}}_1 = [a_{ast} \frac{1 - e^2}{1 + e \cos \nu(t)} \quad 0 \quad 0]^T \tag{24}$$

and the new spacecraft position is found by

$$\tilde{\boldsymbol{R}}' = \tilde{\boldsymbol{R}} + \tilde{\boldsymbol{r}}_1 \tag{25}$$

with a_{ast} the asteroid's semi-major axis (in AU), e the eccentricity of the asteroid's orbit around the Sun and $\nu(t)$ the asteroid's true anomaly at time t. The position is then rotated by a sequence of rotation matrices

$$\tilde{\boldsymbol{r}}_I = \mathbb{T}_z(\mathbf{RAAN}_{ast}) \mathbb{T}_x(i_{ast}) \mathbb{T}_z(\omega_{ast}) \mathbb{T}_z(\nu) \tilde{\boldsymbol{R}}' \tag{26}$$

where $\mathbf{RAAN}_{ast}$ is the right ascension of the ascending node of the asteroid's orbit, i_{ast} the inclination of the asteroid's orbit and ω_{ast} the argument of periapsis of the asteroid's orbit.

For the spacecraft's velocity in the inertial heliocentric frame, the velocity of the asteroid's frame needs to be taken into account [30]. The angular momentum H of that frame is given by

$$H = \sqrt{\mu_{Sun} a_{ast} (1 - e^2)} \tag{27}$$

Then, the velocity of the asteroid's frame in the radial direction is

$$\dot{\tilde{r}}_1 = \frac{\mu_{Sun}}{H} e \sin \nu \tag{28}$$

and in the tangential direction

$$\tilde{r}_1\Omega = \frac{\mu_{Sun}}{H}(1 + e\cos\nu) \tag{29}$$

From Kepler's second equation,

$$\Omega = n_{ast}\frac{a_{ast}}{\tilde{r}_1^2}\sqrt{(1-e^2)} \tag{30}$$

with n_{ast} the mean motion of the asteroid.

Incorporating the velocity of the asteroid's moving frame gives for the spacecraft velocity

$$\dot{\tilde{\boldsymbol{R}}}' = \dot{\tilde{R}} + \begin{bmatrix}\dot{\tilde{r}}_1 & \tilde{r}_1\Omega & 0\end{bmatrix} + \begin{bmatrix}0 & 0 & \Omega\end{bmatrix} \times \tilde{\boldsymbol{R}} \tag{31}$$

Lastly, the velocity of the spacecraft in the inertial heliocentric frame then needs to be rotated,

$$\dot{\tilde{\boldsymbol{r}}}_I = \mathbb{T}_z(\mathbf{RAAN}_{ast})\mathbb{T}_x(i_{ast})\mathbb{T}_z(\omega_{ast})\mathbb{T}_z(\nu)\dot{\tilde{\boldsymbol{R}}}' \tag{32a}$$

Transforming the dimensionless time t_{EH} of the EH3BP to the dimensional time $\tilde{t}$ of the SS2BP is not as straightforward, as there is no

$$t'_{EH} = t \mod 2\pi \tag{33a}$$

$$E = 2(\arctan\left[\left(\frac{1+e_{ast}}{1-e_{ast}}\right)^{-0.5}\tan(\frac{t'_{EH}}{2})\right]) + 2\pi \mod 2\pi \tag{33b}$$

$$M = E - e_{ast}\sin(E) + \lfloor\frac{t_{EH}}{2\pi}\rfloor 2\pi; \tag{33c}$$

$$\tilde{t} = M\frac{180}{\pi}\frac{1}{n_{ast}} + T_p \tag{33d}$$

where E is the eccentric anomaly, M is the mean anomaly and T_p is the time of perihelion passage (31-10-2021 23:40).

IV. Optimal Control

Optimizing the trajectories is done by formulating an optimal control problem, which is described in Section IV.A. This problem is solved using a direct pseudo-spectral collocation method, as described in Section IV.B.

A. Optimal Control Problem Description

A trajectory can be described as the state of the spacecraft

$$s(t) = [\ x \quad y \quad z \quad \dot{x} \quad \dot{y} \quad \dot{z}\ ]^T \tag{34}$$

and its control

$$\begin{bmatrix} 0^\circ & -180^\circ \end{bmatrix}^T \leq \boldsymbol{u}(t) = \begin{bmatrix} \alpha & \delta \end{bmatrix}^T \leq \begin{bmatrix} 90^\circ & 180^\circ \end{bmatrix}^T \tag{35}$$

or,

$$\begin{bmatrix} -1 & -1 & -1 \end{bmatrix}^T \leq \boldsymbol{u}(t) = \begin{bmatrix} n_x & n_y & n_z \end{bmatrix}^T \leq \begin{bmatrix} -1 & -1 & -1 \end{bmatrix}^T \tag{36}$$

as a function of time. The objective of the optimal control problem for a time-optimal trajectory is to find the state and control over time such that they abide by the dynamics described in Section III and minimize the objective function

$$J = t_f - t_0 \tag{37}$$

where t_0 and t_f are the trajectory's initial and final time, respectively.

1. Phases

The optimal control problem is solved separately for the outbound and inbound trajectory. For each phase of those trajectories, the appropriate constraints are chosen to match its dynamical model. The phases are referenced using subscript $_{\text{O1/2/3}}$ for the outbound trajectory and $_{\text{I1/2/3}}$ for the inbound trajectory.

The phases have to be connected smoothly by setting constraints on the initial and final time and state of the trajectory. This will guarantee continuity across the connection points in terms of the time, position and velocity of the spacecraft. Ideally, the control is also connected at the connection points but in this work this is not enforced. The time of flight is long enough to recalculate the control connection in future higher fidelity analysis of the trajectories.

The states and time of the CR3BP and EH3BP are first transformed to the heliocentric inertial frame through the steps described in Section III.E before being connected to the SS2BP. Again, the tilde notation $\tilde{(\cdot)}$ is used to denote a parameter (or vector) in dimensional units. The state vector connection constraints are given by

$$\tilde{\boldsymbol{s}}_{f,\text{O1}} = \tilde{\boldsymbol{s}}_{0,\text{O2}} \tag{38a}$$

$$\tilde{\boldsymbol{s}}_{f,\text{O2}} = \tilde{\boldsymbol{s}}_{0,\text{O3}} \tag{38b}$$

$$\tilde{\boldsymbol{s}}_{f,\text{I1}} = \tilde{\boldsymbol{s}}_{0,\text{I2}} \tag{38c}$$

$$\tilde{\boldsymbol{s}}_{f,\text{I2}} = \tilde{\boldsymbol{s}}_{0,\text{I3}} \tag{38d}$$

and the time connection constraints are given by

$$\tilde{t}_{f,\text{O1}} = \tilde{t}_{0,\text{O2}} \tag{39a}$$

$$\tilde{t}_{f,\mathrm{O2}} = \tilde{t}_{0,\mathrm{O3}} \tag{39b}$$

$$\tilde{t}_{f,\mathrm{I1}} = \tilde{t}_{0,\mathrm{I2}} \tag{39c}$$

$$\tilde{t}_{f,\mathrm{I2}} = \tilde{t}_{0,\mathrm{I3}} \tag{39d}$$

For both the outbound and the inbound trajectory, 14 connection constraints are enforced to ensure proper connection.

2. Boundary constraints

The following boundary constraints are set up to ensure the spacecraft departs from the Sun-Earth L_2 point and arrives at the Sun-asteroid L_1 point for the outbound trajectory and vice versa for the inbound trajectory.

$$\boldsymbol{s}_{0,\mathrm{O1}} = \boldsymbol{s}_{\mathrm{SE-L2}} \tag{40a}$$

$$\boldsymbol{s}_{f,\mathrm{O3}} = \boldsymbol{s}_{\mathrm{Sa-L1}} \tag{40b}$$

$$\boldsymbol{s}_{0,\mathrm{I1}} = \boldsymbol{s}_{\mathrm{Sa-L1}} \tag{41a}$$

$$\boldsymbol{s}_{f,\mathrm{I3}} = \boldsymbol{s}_{\mathrm{SE-L2}} \tag{41b}$$

The values for the state vectors of the spacecraft at the $\mathrm{SE-L2}$ point and the $\mathrm{Sa-L1}$ point are given in Table 4.

Table 4 Coordinates and velocities at the Lagrange points $\mathrm{SE-L2}$ **and** $\mathrm{Sa-L1}$**. Note that the coordinates are made dimensionless with respect to the CR3BP and EH3BP, respectively.**

Location	x	y	z	$\dot{x}$	$\dot{y}$	$\dot{z}$
SE – L2	1.010034116	0.0	0.0	0.0	0.0	0.0
Sa – L1	$-\left(\frac{1}{3}\right)^{1/3}$	0.0	0.0	0.0	0.0	0.0

3. Path constraints

The following path constraints are set up for the control vector throughout the entire cycle trajectory. First, the norm of the control vector is enforced to be unity

$$\|\boldsymbol{u}\| = 1 \tag{42}$$

Secondly, the control vector always has to point away from the sun, since a solar sail cannot generate acceleration towards the Sun [3],

$$\hat{\boldsymbol{r}}_1 \cdot \hat{\boldsymbol{n}} \geq 0 \tag{43}$$

B. PSOPT

To solve the optimal control problem, this work uses open source software package PSOPT, a direct pseudospectral collocation method [31]. This method discretizes the time interval into a finite number collocation points and uses Legendre-Chebyshev polynomials to interpolate the time dependent variables at the collocation points. This transforms the infinite dimensional optimal control problem into a finite dimensional Non-Linear Programming (NLP) problem.

This type of method does require a sufficiently accurate initial guess. These will first have to be generated, as is described in the next chapter.

V. Initial Guess Generation

The initial guess for PSOPT is generated with a genetic algorithm. The outbound and inbound trajectories are generated separately. The algorithm is designed based on the MMR for generality. That way, the methodology is applicable to any asteroid, instead of only to ones that are nearly circular and nearly coplanar with Earth. The cycle time $T_{cyc} = k_2$y follows directly from the MMR (see Equation 3), where the value for k_2 is equal to the number of complete orbits of Earth in a cycle. The MMR of Earth : 2001AE2 is $n_{ast} : n_{Earth} = 7 : 11$, giving a cycle time of $T_{cyc} = 11$y. For the outbound trajectory, the search space for the departure date consists of one full cycle time and is set from 01-01-2030 to 01-01-2041.

Finally, although the genetic algorithm is designed based on the MMR, the results are also compatible with the synodic period for this asteroid. The only difference here is that the dwelling time at the end of the cycle is increased slightly, which for this asteroid results in a slightly worse mismatch between the initial and final conditions of the cycle (i.e., delay of the Earth's position).

A. Genetic Algorithm

A genetic algorithm is used to search for a suboptimal outbound and inbound trajectory. Both trajectories are separated into two parts: the CR3BP and a combined SS2BP+EH3BP part. The EH3BP is attached to the SS2BP to limit the number of design variables. Furthermore, because the EH3BP is only valid close to the asteroid, it has been assigned a fixed time of 90 days, based on the approximate distance traveled from the asteroid after that time found by trial and error. At that point the distance of the spacecraft is at most approximately ≈ 25 dimensionless units in the EH3BP, which for 2001AE is equal to ≈ 2000km. For sake of ease in the implementation in the algorithm, the EH3BP has been assigned a fixed time instead of a fixed maximum spacecraft distance from the asteroid.

The genetic algorithm searches for a connection point between the CR3BP and the SS2BP with a minimal discontinuity in the position and velocity of the state. This is done using a fitness function of the form

$$J = \Delta R + s_v \Delta V \tag{44}$$

where ΔR and ΔV are the error in position and velocity, respectively, and s_v is a scale value. For this scale value a range of nine values between 1×10^4 to 5×10^6 is used. Varying the scale value did not lead to consistently better or worse times of flight. The found trajectories are suboptimal as the sail orientation is assumed constant over the CR3BP and combined SS2BP+EH3BP parts. The genetic algorithm tries to find these trajectories by varying the following chromosome

$$\boldsymbol{g} = [\begin{array}{ccccccc} \alpha_{\text{CR}} & \alpha_{\text{SS}} & \delta_{\text{CR}} & \delta_{\text{SS}} & t_D & t_C & t_A \end{array}]^T \tag{45}$$

For the outbound trajectory, the genes in the chromosome are given by

- $0° \leq \alpha_{\text{CR}} \leq 90°$: the cone angle in the CR3BP
- $0° \leq \alpha_{\text{SS}} \leq 90°$: the cone angle in the SS2BP+EH3BP
- $-180° \leq \delta_{\text{CR}} \leq 180°$: the clock angle in the CR3BP
- $-180° \leq \delta_{\text{SS}} \leq 180°$: the clock angle in the SS2BP+EH3BP
- $01 - 01 - 2030 \leq t_D \leq 01 - 01 - 2041$: the departure time for the CR3BP
- $T_{cyc}/8 \leq t_C \leq 3T_{cyc}/8$: the time of flight for the CR3BP up until connection with the SS2BP
- $T_{cyc}/4 \leq t_A \leq T_{cyc}/2$: the arrival time of flight of the trajectory

After the outbound trajectory is generated and its arrival time of flight $t_{A,O}$ is found, the inbound trajectory is searched for by adjusting the bounds for the time genes as follows:

- $t_{A,O} \leq t_D \leq t_{A,O} + T_{cyc}/4$: the departure time for the EH3BP
- $T_{cyc}/8 \leq t_C \leq 3T_{cyc}/8$: the time of flight for the EH3BP+SS2BP up until connection with the CR3BP
- $T_{cyc}/4 \leq t_A \leq T_{cyc} - t_{A,O}$: the arrival time of flight of the trajectory

The genetic algorithm used a population size of 70 and evolved the population for 50 generations. This was done for 10 different seeds to decrease the influence of outliers (due to randomness) in the initial population on the result of the algorithm. The algorithm employs often-used techniques such as a tournament style selection procedure (more specifically, a binary tournament), crossover, mutation and elitism (4% of the population). Specific values for the settings of a genetic algorithm depend on the nature of the optimization problem and were therefore searched for by trial and error. For example, the overall fitness of the population did not decrease much after 50 generations, so that value was chosen for the algorithm.

B. Initial Guess Results

The best results of the initial guess trajectories generated by the genetic algorithm are shown in Figure 8 and Figure 9, for the outbound and inbound phases respectively. The numerical results for both phases are given in Table 5.

The outbound trajectory's first phase (CR3BP) has a cone angle of $\alpha_{CR} = 54.3°$ and a clock angle of $\delta_{CR} = 84.7°$. This results in the sail normal vector pointing mostly in the $x - y$ plane and only slightly towards the positive z direction.

This can be seen in the top part of Figure 8d. Most of the plane change is done in phase $O_{2,3}$, where the cone angle is $\alpha_{SS} = 77.6°$ and the clock angle is $\delta_{SS} = 145.5°$ resulting in a mostly out-of-plane force vector.

The time of flight for the outbound trajectory is 4.18 years, starting from SE – L2 on 01 – 12 – 2035 and arriving at Sa – L1 on 04 – 02 – 2040. The connection point between the CR3BP and the SS2BP has a discontinuity in position of $\Delta R = 6.018 \times 10^5$km and in velocity of 1.464km/s. In the non-dimensional units of the CR3BP, this translates to a position discontinuity of 4.023×10^{-3} and a velocity discontinuity of 4.913×10^{-2}. This is small enough for PSOPT to find an optimal trajectory.

The inbound trajectory's first phase (EH3BP+SS2BP) has a cone angle of $\alpha_{SS} = 24.4°$ and a clock angle of $\delta_{SS} = -43.3°$. Phase I_3 (CR3BP) has a cone angle of $\alpha_{CR} = 65.3°$ and a clock angle of $\delta_{CR} = -146.5°$. Both phases have an out-of-plane sail normal vector and the plane change is distributed more evenly over both phases.

The time of flight for the inbound trajectory is 3.75 years, starting from Sa – L1 on 29 – 09 – 2042 and arriving at SE – L2 on 30 – 06 – 2046. The connection point between the SS2BP and the CR3BP has a discontinuity in position of $\Delta R = 2.451 \times 10^5$km and in velocity of 4.334km/s. In the non-dimensional units of the CR3BP, this translates to a position discontinuity of 1.638×10^{-3} and a velocity discontinuity of 1.455×10^{-1}. Although the velocity mismatch here is much larger, these are also found to be small enough for PSOPT to optimize the trajectory.

Recall from Section II.A that this work uses the synodic period to determine the cycle time for 2001AE, instead of using the MMR between Earth and the asteroid. This does not influence the optimization of the trajectories and only slightly decreases the mismatch at the end of each cycle. The cycle time is therefore given by $T_{cyc} = n_{syn}T_{syn}$, with n_{syn} the lowest number of synodic periods that can fit the total time of flight and $T_{syn} = 2.760$y. The total time of flight is 10.58 years, giving $n_{syn} = 4$ for the number of synodic periods. This results in a cycle time of $T_{cyc} = 11.04$y - slightly more than the 11 years resulting from the MMR.

Table 5 Numerical results for the outbound and inbound initial guess trajectories generated by the genetic algorithm.

	Outbound	Inbound
α_{CR} [deg]	54.3	24.4
δ_{CR} [deg]	84.7	−43.3
α_{SS} [deg]	77.6	65.3
δ_{SS} [deg]	145.5	−146.5
t_D [DD – MM – YYYY]	01 – 12 – 2035	29 – 09 – 2042
t_C [DD – MM – YYYY]	01 – 06 – 2037	21 – 06 – 2045
t_A [DD – MM – YYYY]	04 – 02 – 2040	30 – 06 – 2046
ΔR [km]	6.018×10^5	2.451×10^5
ΔV [km/s]	1.464	4.334
ΔR [−]	4.023×10^{-3}	1.638×10^{-3}
ΔV [−]	4.913×10^{-2}	1.455×10^{-1}

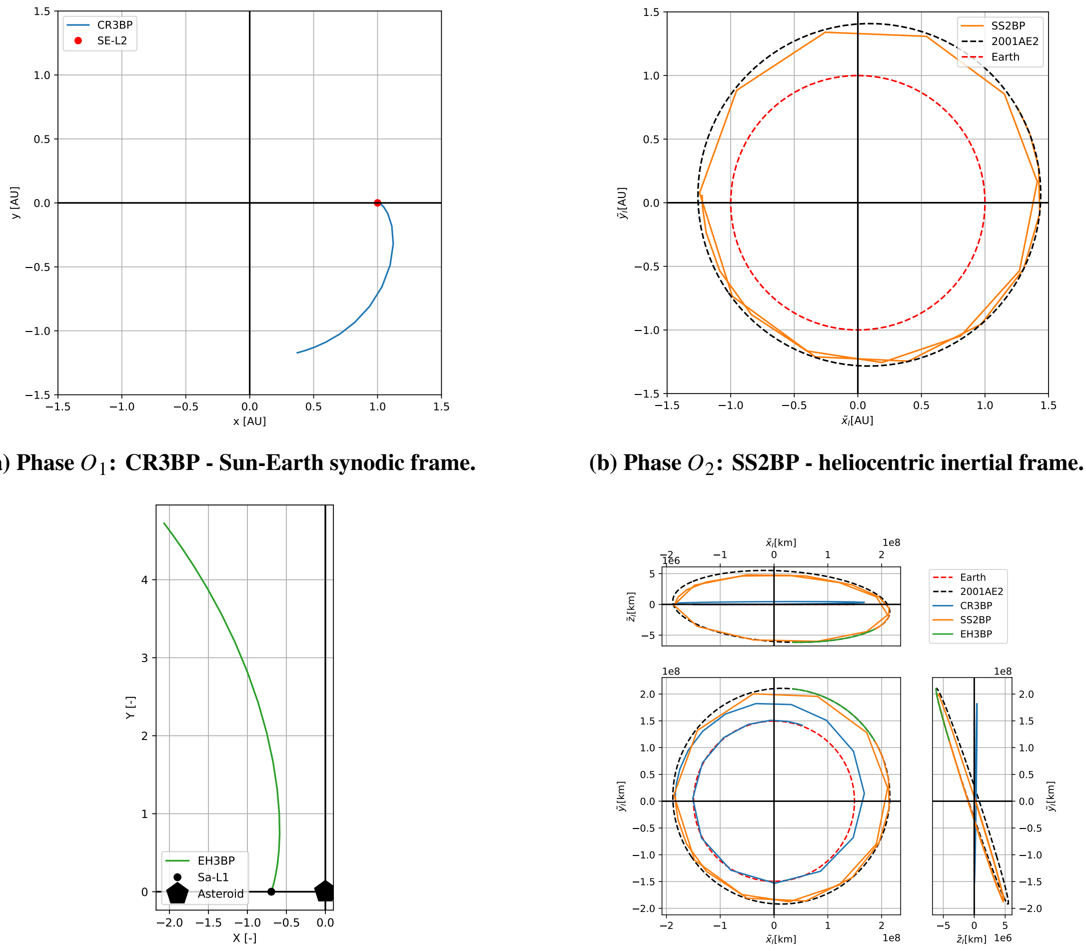

(a) Phase O_1: CR3BP - Sun-Earth synodic frame.

(b) Phase O_2: SS2BP - heliocentric inertial frame.

(c) Phase O_3: EH3BP - Sun-asteroid synodic frame.

(d) Phase $O_{1,2,3}$: 3D heliocentric view.

Fig. 8 The initial guess results of the outbound trajectory: a) Phase O_1 in the Sun-Earth synodic frame, b) Phase O_2 in the heliocentric inertial frame, c) Phase O_3 in the Sun-asteroid synodic frame, and d) the complete initial guess trajectory in the heliocentric inertial frame.

The dwell time at Sa – L1 between the outbound and inbound trajectory is 2.65 years. The difference between the cycle time and the total time of flight results in a dwell time of 0.46 years at SE – L2 at the end of the inbound trajectory and before the start of the next cycle.

VI. Results

The results from PSOPT are shown in Figure 10 and Figure 11 for the outbound and inbound trajectory, respectively. The numerical results for the departure, connection and arrival times of the trajectories and the position and velocity mismatch at the connection points are listed in Table 6. The control profiles are shown in Figure 12.

In Table 6, the connection points are labelled $C1$ and $C2$ in order of appearance during the trajectory. For the outbound trajectory, connection point $C1$ is the connection between the CR3BP and the SS2BP, whereas connection

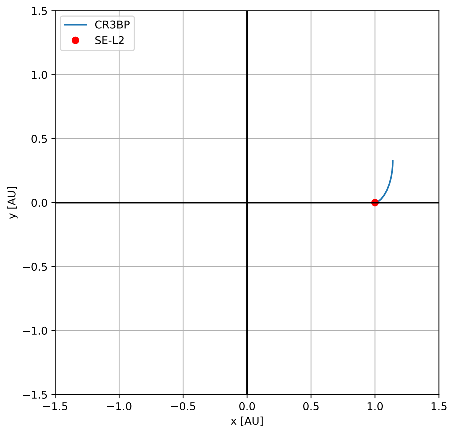

(a) Phase I_3: CR3BP - Sun-Earth synodic frame.

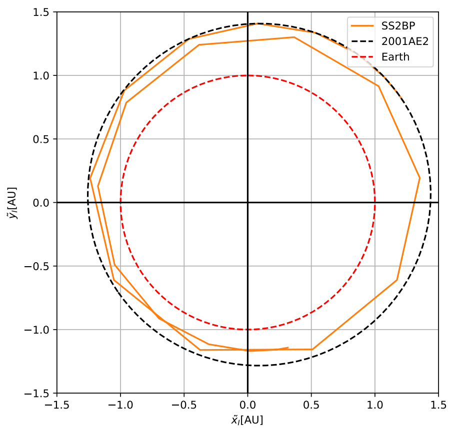

(b) Phase I_2: SS2BP - heliocentric inertial frame.

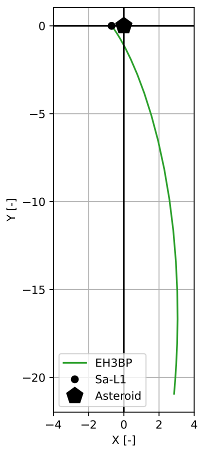

(c) Phase I_1: EH3BP - Sun-asteroid synodic frame.

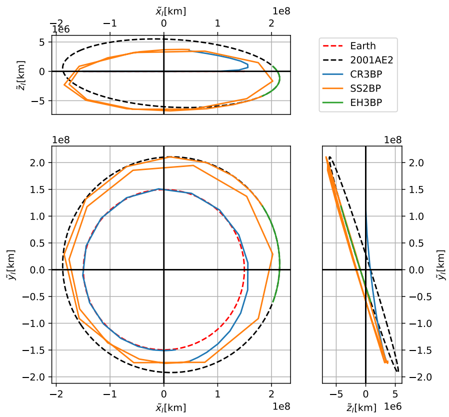

(d) Phase $I_{1,2,3}$: 3D heliocentric view.

Fig. 9 The initial guess results of the inbound trajectory: a) Phase I_3 in the Sun-Earth synodic frame, b) Phase I_2 in the heliocentric inertial frame, c) Phase I_1 in the Sun-asteroid synodic frame, and d) the complete initial guess trajectory in the heliocentric inertial frame.

point $C2$ is the connection between the SS2BP and the EH3BP. For the inbound trajectory, connection point $C1$ is the connection between the EH3BP and the SS2BP, whereas connection point $C2$ is the connection between the SS2BP and the CR3BP.

The time of flight for both trajectories is significantly shorter compared to the initial guess trajectories. For the outbound trajectory, this is a reduction of 26%, whereas for the inbound trajectory this is a reduction of 29%. This means that the dwelling time at $\mathrm{Sa-L1}$ and $\mathrm{SE-L2}$ are also significantly longer. For the solution found by PSOPT, the dwelling times at $\mathrm{Sa-L1}$ increased from 967 days (2.65 years) to 1585 days (4.34 years).The dwelling time at $\mathrm{SE-L2}$ increased from 168 days (0.46 years) to 351 days (0.95 years).

The absolute mismatch in the position and velocity at the connection points is similar for all four connection points. However, because of the significant difference in the time and length scales of the CR3BP and EH3BP, these

Table 6 Numerical results for the outbound and inbound trajectories generated by PSOPT.

	Outbound	Inbound
t_D [DD – MM – YYYY]	01 – 03 – 2036	04 – 08 – 2043
t_{C1} [DD – MM – YYYY]	31 – 08 – 2037	23 – 08 – 2043
t_{C2} [DD – MM – YYYY]	27 – 01 – 2039	29 – 03 – 2045
t_A [DD – MM – YYYY]	02 – 04 – 2039	31 – 03 – 2046
tof_1 [d]	548.0	18.9
tof_2 [d]	513.9	585.4
tof_3 [d]	65.1	365.0
tof [d]	1127.0	969.3
ΔR_{C1} [km]	6.434×10^4	2.455×10^3
ΔV_{C1} [km/s]	1.459×10^{-2}	3.332×10^{-4}
ΔR_{C2} [km]	4.709×10^4	5.531×10^4
ΔV_{C2} [km/s]	8.015×10^{-3}	9.430×10^{-3}
ΔR_{C1} [−]	4.300×10^{-4}	3.049×10^1
ΔV_{C1} [−]	4.898×10^{-4}	3.250×10^1
ΔR_{C2} [−]	5.848×10^2	3.698×10^{-4}
ΔV_{C2} [−]	7.837×10^2	3.166×10^{-4}

discontinuities are much larger in the non-dimensional units of the EH3BP than in the non-dimensional units of the CR3BP. Since the connection point of the asteroid is much closer to the asteroid (up to a few hundred kilometers from the asteroid), a position mismatch on the order of thousands of kilometers is also a lot more significant. However, as mentioned before, the dwelling time at Sa – L1 is relatively long and can be used in future studies to refine the connection between the EH3BP and the SS2BP for both the outbound and inbound trajectories. Furthermore, it is important to recall that an increase of ≈ 10% can be expected when using non-ideal sail models, based on the results of Reference [11].

The control profile of the sail is smooth for the CR3BP and the EH3BP, but significantly less smooth for the SS2BP. An extra term was added in the objective function in an attempt to smoothen the results. By including an integral cost function based on the derivatives of the control states, the change in the sail orientation is minimized over the entire trajectory. This new cost function is given by

$$J = t_f - t_0 + \int_{t_0}^{t_f} \left[\dot{n}_x(t)^2 + \dot{n}_y(t)^2 + \dot{n}_z(t)^2 \right] dt \tag{46}$$

where $\dot{n}_{x,y,z}$ are the time derivatives of the control vector components (i.e., orientation of the sail normal). Whereas this helped smoothen the control profile for all three phases of the trajectory without affecting the time of flight significantly, PSOPT was unable to find a trajectory with a smoother profile for the SS2BP.

The results from PSOPT are verified by reintegrating the trajectories from the initial state over time with an

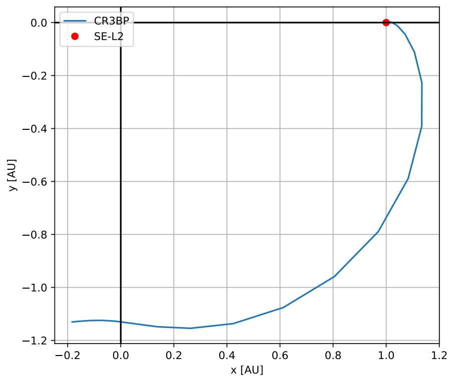

(a) CR3BP - Sun-Earth synodic frame.

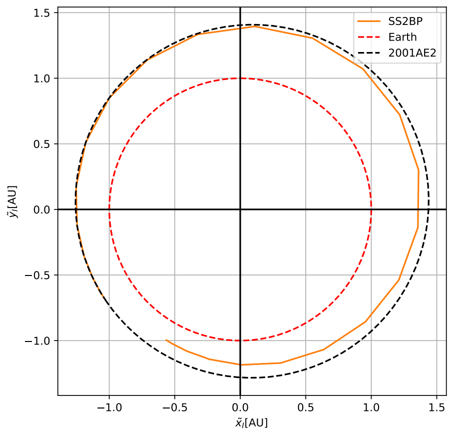

(b) SS2BP - heliocentric inertial frame.

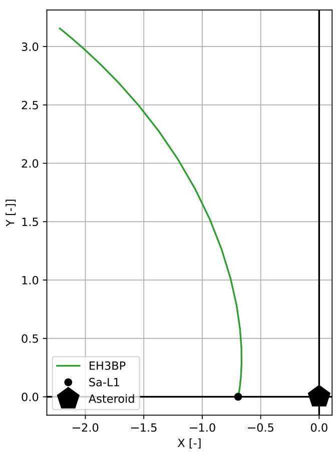

(c) EH3BP - Sun-asteroid synodic frame.

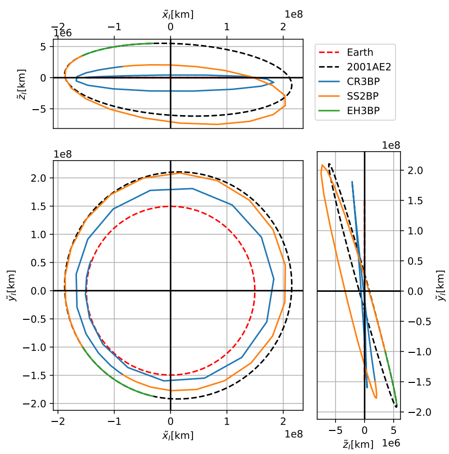

(d) 3D heliocentric view.

Fig. 10 The optimal trajectory results from PSOPT: a) the CR3BP in the Sun-Earth synodic frame, b) the SS2BP in the heliocentric inertial frame, c) the EH3BP in the Sun-asteroid synodic frame, and d) the complete initial guess trajectory in the heliocentric inertial frame.

interpolated control profile, shown in Figure 13. The resulting reintegrated trajectories accurately match the results from PSOPT, indicating that the PSOPT trajectories match the models over the entire trajectory and not just on the collocation nodes. This indicates that the control profile of the SS2BP is smooth enough to accurately follow the model, even though it is likely not the most optimal solution.

VII. Conclusion

The time-optimal trajectories show that a cycler can be set up to asteroid 2001AE2 within the cycle time $T_{cyc} = 11.04$y using near-future solar sail technology (i.e., a lightness number of $\beta = 0.05$). The asteroid shows a close mean-motion resonance (MMR) of almost $n_{ast} : n_{Earth} = 7 : 11$ (with n the mean motion of the body), indicating that within one cycle the asteroid completes 7 orbits and Earth completes 11 orbits (though there is a small delay in Earth's position).

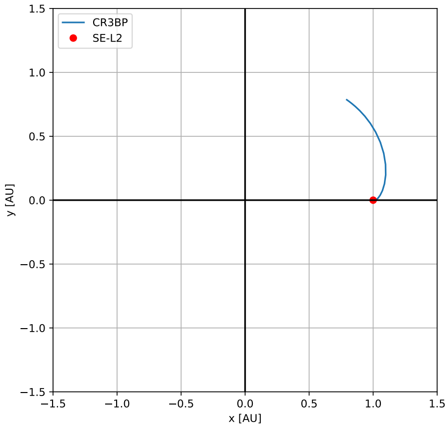

(a) CR3BP - Sun-Earth synodic frame.

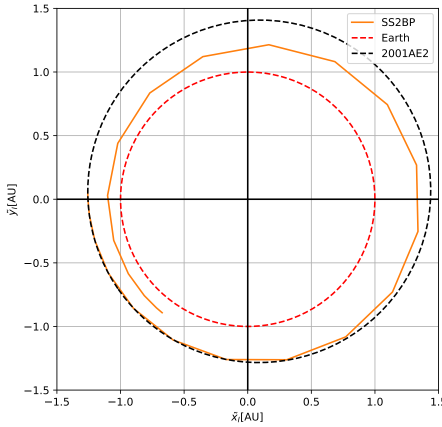

(b) SS2BP - heliocentric inertial frame.

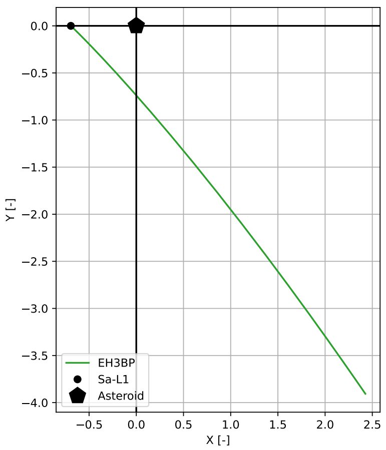

(c) EH3BP - Sun-asteroid synodic frame.

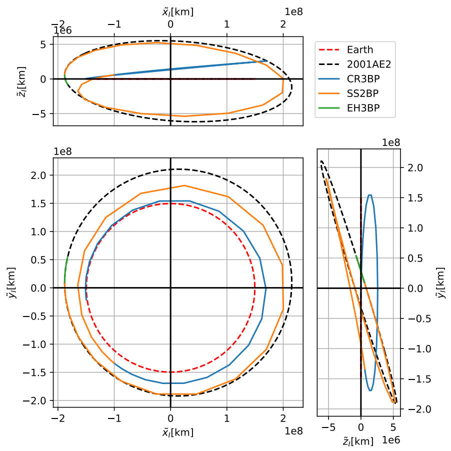

(d) 3D heliocentric view.

Fig. 11 The optimal trajectory results from PSOPT: a) the CR3BP in the Sun-Earth synodic frame, b) the SS2BP in the heliocentric inertial frame, c) the EH3BP in the Sun-asteroid synodic frame, and d) the complete initial guess trajectory in the heliocentric inertial frame.

An initial cycle is found between Lagrange point 2 (SE – L2) of the Sun-Earth Circular Restricted Three-Body Problem (CR3BP) and Lagrange point 1 (Sa – L1) of the Sun-asteroid Elliptic Hill Three-Body Problem (EH3BP) of asteroid 2001AE2. It departs from SE – L2 on 01 – 03 – 2036 and arrives back at SE – L2 on 17 – 03 – 2047, which can theoretically be repeated indefinitely. The outbound trajectory reaches Sa – L1 after a time of flight of 1127 days (3.08 years) and will stay at Sa – L1 for 1585 days (4.34 years). The inbound trajectory reaches SE – L2 after a time of flight of 969 days (2.65 years) and will stay there for 351 days (0.95 years).

There's a mismatch in the position and velocity of the connections between CR3BP and the Sun-sail Two-Body Problem (SS2BP) with an acceptable dimensionless size of $\tilde{\times}10^{-4}$. This translates to a dimensional size on the order of $\delta R\tilde{\times}10^{4}$km and $\delta V\tilde{\times}10^{-2}$km/s. For the mismatch in the position and velocity of the connections between the EH3BP and SS2BP the dimensional size is similar (or even better). However, because the time and length scales of the EH3BP

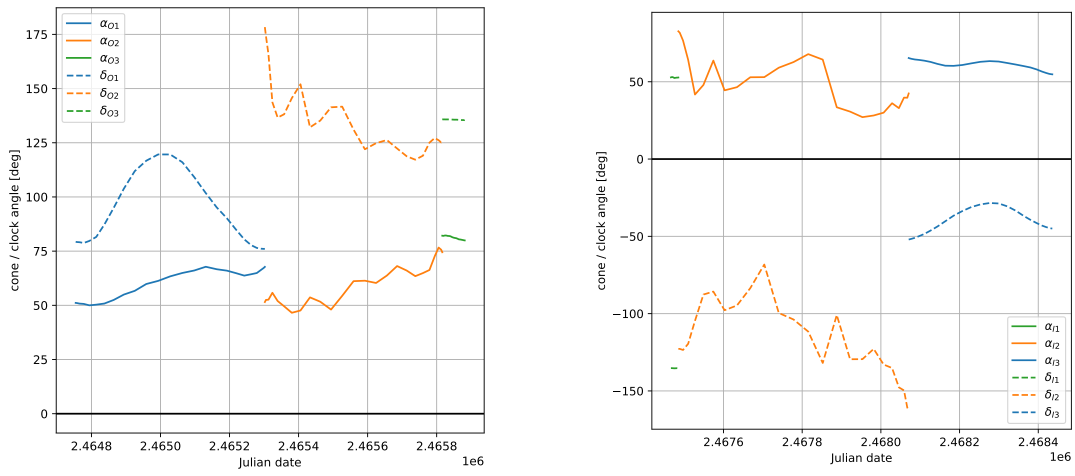

(a) Outbound trajectory. **(b) Inbound trajectory.**

Fig. 12 Control profile for the cone angle α and clock angle δ for the a) outbound and b) inbound trajectory.

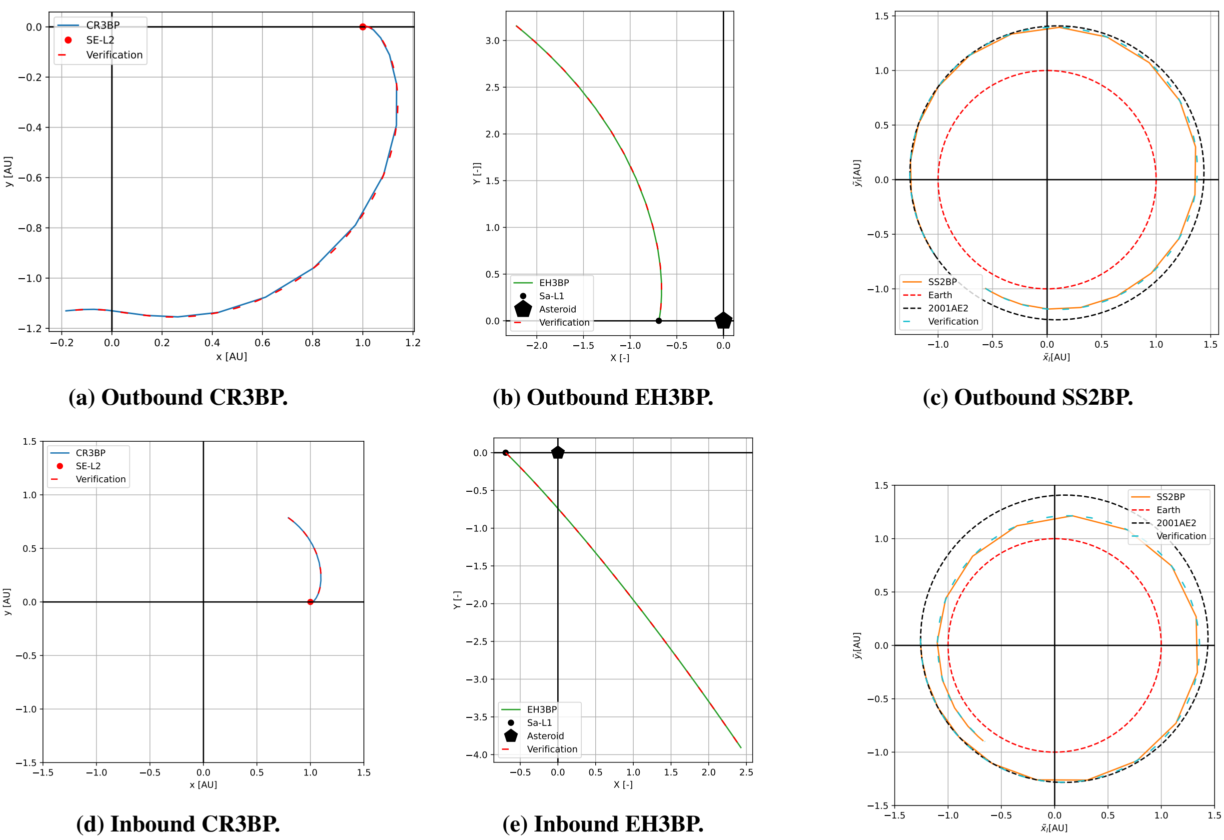

(a) Outbound CR3BP. **(b) Outbound EH3BP.** **(c) Outbound SS2BP.**

(d) Inbound CR3BP. **(e) Inbound EH3BP.**

Fig. 13 Verification of the PSOPT results by reintegration of initial states.

are much smaller, the dimensionless sizes of the mismatch are much larger comparatively. The dwelling time at Sa – L1 is relatively long and can be used in future studies to refine the connection between the EH3BP and the SS2BP for both the outbound and inbound trajectories.

Although asteroid 2001AE2 has an orbit suitable for use with the synodic period, this work shows that the MMR method is a viable option for use with asteroids that are not in an orbit suitable with the synodic period (i.e., asteroids in a non-circular or non-coplanar orbit).

It is important to note that this work makes use of assumptions and simplifications so the results should be interpreted as serving as an initial proof of concept for a solar sail asteroid cycler and not as a finalized trajectory. Currently the spacecraft is assumed to be stationary at $\mathrm{SE}-\mathrm{L2}$ and $\mathrm{Sa}-\mathrm{L1}$ during the dwelling times, but in practice this is unrealistic. The libration points are unstable as a small perturbation will lead the spacecraft to drift away along one of the manifolds. Rather than assume the spacecraft to remain stationary, libration point orbits should be included in the design to fill the dwelling time of the cycle. The CR3BP is an often used model in preliminary trajectory design, but on its own it disregards the gravitational influence of other celestial bodies acting on the spacecraft. Furthermore, simple two-body dynamics are used to model the trajectory in between the CR3BP and the EH3BP. Gravitational influence of other celestial bodies is not incorporated, such as the other inner planets. Future work is also needed to include higher fidelity models for the spacecraft dynamics in close proximity to the asteroid. These could include fourth-body perturbations, and the rotation and shape of the asteroid. Finally, this work uses an ideal sail model, though a more accurate representation of the solar sail would be given by taking optical and parametric sail force models and sail degradation into account.

References

[1] Mori, O., Shirasawa, Y., Mimasu, Y., Tsuda, Y., Sawada, H., Saiki, T., Yamamoto, T., Yonekura, K., Hoshino, H., Kawaguchi, J., and Funase, R., "Overview of IKAROS Mission," *Advances in Solar Sailing*, edited by M. Macdonald, Springer Berlin Heidelberg, 2014, pp. 25–43. https://doi.org/10.1007/978-3-642-34907-2_3.

[2] Spencer, D. A., Betts, B., Bellardo, J. M., Diaz, A., Plante, B., and Mansell, J. R., "The LightSail 2 solar sailing technology demonstration," *Advances in Space Research*, 2020. https://doi.org/10.1016/j.asr.2020.06.029.

[3] McInnes, C. R., *Solar Sailing Technology, Dynamics and Mission Applications*, Springer-Verlag, 1999.

[4] Heaton, A., Ahmad, N., and Miller, K., "Near Earth Asteroid Scout Solar Sail Thrust and Torque Model," *4th International Symposium on Solar Sailing*, 2017, pp. 1–10.

[5] Heiligers, J., Mingotti, G., and Mcinnes, C., "OPTIMISATION OF SOLAR SAIL INTERPLANETARY HETEROCLINIC CONNECTIONS," *2nd IAA Conference on Dynamics and Control of Space Systems - DyCoSS*, 2014.

[6] Heiligers, J., Fernandez, J. M., Stohlman, O. R., and Wilkie, W. K., "Trajectory design for a solar-sail mission to asteroid 2016 HO3," *Astrodynamics*, Vol. 3, No. 3, 2019, pp. 231–246. https://doi.org/10.1007/s42064-019-0061-1.

[7] Vergaaij, M., “Time-optimal solar sail transfers from Earth to pole-sitters at Mars and Venus,” Msc thesis, Delft University of Technology, 2018.

[8] Hollister, W. M., “Periodic orbits for interplanetary flight.” *Journal of Spacecraft and Rockets*, Vol. 6, No. 4, 1969, pp. 366–369. https://doi.org/https://doi.org/10.2514/3.29664.

[9] Aldrin, E. E., “Cyclic Trajectory Concepts,” , 1985.

[10] Heiligers, J., Mingotti, G., and McInnes, C. R., “Optimal solar sail transfers between Halo orbits of different Sun-planet systems,” *Advances in Space Research*, Vol. 55, No. 5, 2015, pp. 1405–1421. https://doi.org/10.1016/j.asr.2014.11.033, URL http://dx.doi.org/10.1016/j.asr.2014.11.033.

[11] Vergaaij, M., and Heiligers, J., “Time-optimal solar sail heteroclinic-like connections for an Earth-Mars cycler,” *Acta Astronautica*, Vol. 152, No. August, 2018, pp. 474–485. https://doi.org/10.1016/j.actaastro.2018.08.008.

[12] Badescu, V., *Asteroids Prospective Energy and Material Resources*, Springer, 2013. https://doi.org/10.1007/978-3-642-39244-3.

[13] Burbine, T. H., *ASTEROIDS Astronomical and Geological Bodies*, Cambridge Univesity Press, 2017. https://doi.org/10.1017/9781316156582.

[14] ESA, and van der Hucht, K. A., “NEO Chronology,” , 2023. URL http://neo.ssa.esa.int/neo-chronology.

[15] Tricarico, P., “The near-Earth asteroid population from two decades of observations,” *Icarus*, Vol. 284, 2017, pp. 416–423. https://doi.org/10.1016/j.icarus.2016.12.008.

[16] Tholen, D. J., “Asteroid taxonomic classifications,” *Asteroids II*, edited by R. P. Binzel, T. Gehrels, and M. S. Matthews, 1989, pp. 1139–1150.

[17] Bus, S. J., and Binzel, R. P., “Phase II of the Small Main-Belt Asteroid Spectroscopic Survey,” *Icarus*, Vol. 177, 2002, pp. 146–177. https://doi.org/10.1006/icar.2002.6856.

[18] Cellino, A., Bus, S. J., Doressoundiram, A., and Lazzaro, D., “Spectroscopic Properties of Asteroid Families,” *Asteroids III*, edited by W. F. Bottke, A. Cellino, P. Paolicchi, and R. P. Binzel, The University of Arizona Press, 2002, pp. 633–643.

[19] Harris, A. W., and Harris, A. W., “On the Revision of Radiometric Albedos and Diameters of Asteroids,” *Icarus*, Vol. 454, 1997, pp. 450–454. https://doi.org/https://doi.org/10.1006/icar.1996.5664.

[20] Mengali, G., and Quarta, A. A., “Solar sail near-optimal circular transfers with plane change,” *Journal of Guidance, Control, and Dynamics*, Vol. 32, No. 2, 2009, pp. 456–463. https://doi.org/10.2514/1.38079.

[21] Binzel, R. P., Perozzi, E., Rivkin, A. S., Rossi, A., Harris, A. W., Bus, S. J., Valsecchi, G. B., and Slivan, S. M., “Dynamical and compositional assessment of near-Earth object mission targets,” *Meteoritics and Planetary Science*, Vol. 39, No. 3, 2004, pp. 351–366. https://doi.org/10.1111/j.1945-5100.2004.tb00098.x.

[22] NASA/JPL CNEOS, "NASA/JPL Small Body Database," , 2023. URL https://ssd.jpl.nasa.gov/?tools.

[23] Dr. David R. Williams, "Mars Fact Sheet," , 2023. URL https://nssdc.gsfc.nasa.gov/planetary/factsheet/marsfact.html.

[24] Szebehely, V., *Theory of orbits: The restricted problem of three bodies*, Academic Press, 1967.

[25] Biddy, C., and Svitek, T., "LightSail-1 solar sail design and qualification," *Proceedings of the 41st Aerospace Mechanisms Symposium*, Jet Propulsion Lab., National Aeronautics and Space Administration Pasadena, CA, 2012, pp. 451—-463.

[26] Dachwald, B., "Optimal Solar Sail Trajectories for Missions to the Outer Solar System," *Journal of Guidance, Control, and Dynamics*, Vol. 28, No. 6, 2005, pp. 1187–1193. https://doi.org/10.2514/1.13301.

[27] Scheeres, D. J., *Orbital Motion in Strongly Perturbed Environments; Applications to Asteroid, Comet and Planetary Satellite Orbiters*, Springer-Verlag Berlin Heidelberg, 2012. https://doi.org/10.1007/978-3-642-03256-1.

[28] Farrés, A., and Jorba, A., "Orbital Dynamics of a Solar Sail Near L1 and L2 in the Elliptic Hill Problem," *Proceedings of 63rd International Astronautical Congress*, 2012.

[29] Heiligers, J., and Scheeres, D. J., "Solar-sail orbital motion about asteroids and binary asteroid systems," *Journal of Guidance, Control, and Dynamics*, Vol. 41, No. 9, 2018, pp. 1947–1962. https://doi.org/10.2514/1.G003235.

[30] Wakker, K. F., *Fundamentals of Astrodynamics*, Delft University of Technology, 2015.

[31] Becerra, V. M., "Solving complex optimal control problems at no cost with PSOPT," *Proceedings of the IEEE International Symposium on Computer-Aided Control System Design*, IEEE, 2010, pp. 1391–1396. https://doi.org/10.1109/CACSD.2010.5612676.

3

Verification and Validation

This chapter details the verification and validation used to ensure the methodology and the obtained results are correct and optimal. First the dynamical models are covered, then the initial guess generation and finally the PSOPT results are verified.

3.1. Dynamical Models

3.1.1. CR3BP

The CR3BP is verified through several methods. Firstly, the locations of the Lagrange points are verified. These values are listed in Table 3.1 and compared to literature values from [17]. Next, the invariant manifolds are computed both with and without the solar sail force model and compared to results from [7]. The computed manifolds are shown in Figure 3.1 and the literature versions are shown in Figure 3.2 for comparison.

3.1.2. Hill problem

Verification of the Hill problem is done by verification of the locations of the Lagrange points, because there are no manifold trajectories to be found in literature similar to the ones of the CR3BP presented by [7].

The Lagrange points should coincide with their analytic exression of $Sa - L_{1,2} = \left(\pm 3^{-1/3}, 0, 0\right)$. The values for the Lagrange points that are found are $\mathrm{Sa} - \mathrm{L}_{1,2} = (\pm 0.69336127, 0, 0)$, which indeed coincide with their analytic counterparts.

3.2. Initial Guess Generation

To verify the genetic algorithm is able to find a (locally) optimal solution, two simple test functions were implemented: the Himmelblau function and a simple 6-dimensional sphere function. These are much

Table 3.1: Verification of Lagrange point locations in the Sun-Earth system based on literature values from [17].

Lagrange point		x	y	z
L1	Literature	0.989986005	0	0
	Calculated	0.9899860052327467	0	0
L2	Literature	1.010075177	0	0
	Calculated	1.0100751768695142	0	0
L3	Literature	-1.000001267	0	0
	Calculated	-1.000001266834375	0	0
L4	Literature	0.49999696	0.866025404	0
	Calculated	0.4999969595965037	0.866025403785014	-4.49834438e-29
L5	Literature	0.49999696	-0.866025404	0
	Calculated	0.49999695959304635	-0.8660254037870101	-2.14994758e-33

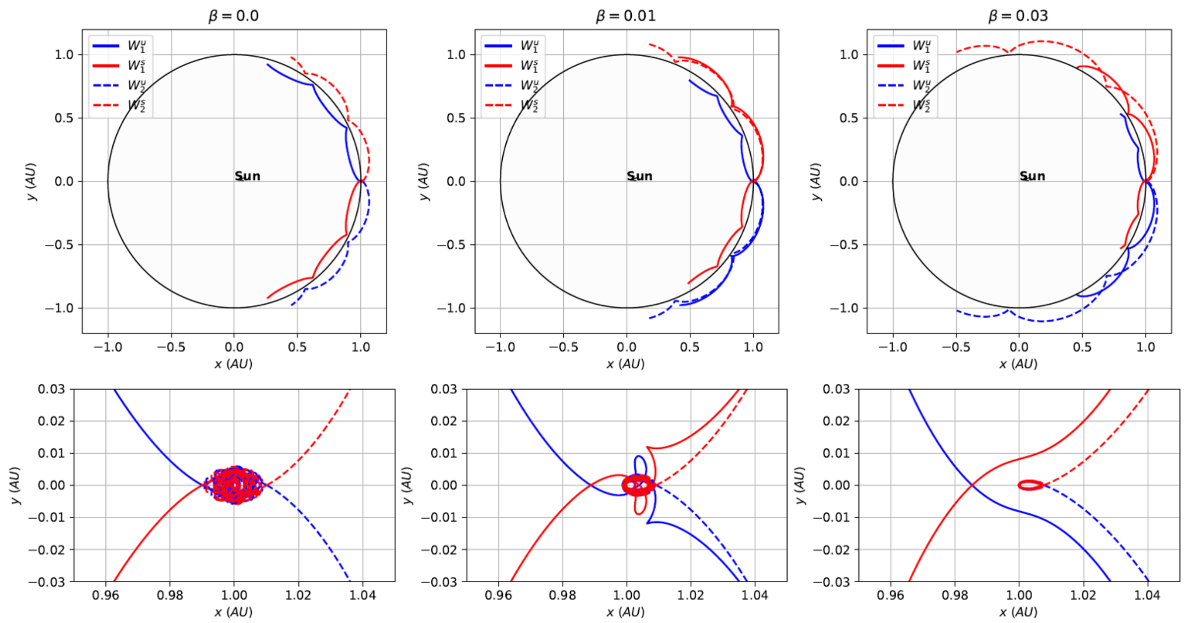

Figure 3.1: Calculated invariant manifolds to verify the implementation of the solar-sail augmented CR3BP.

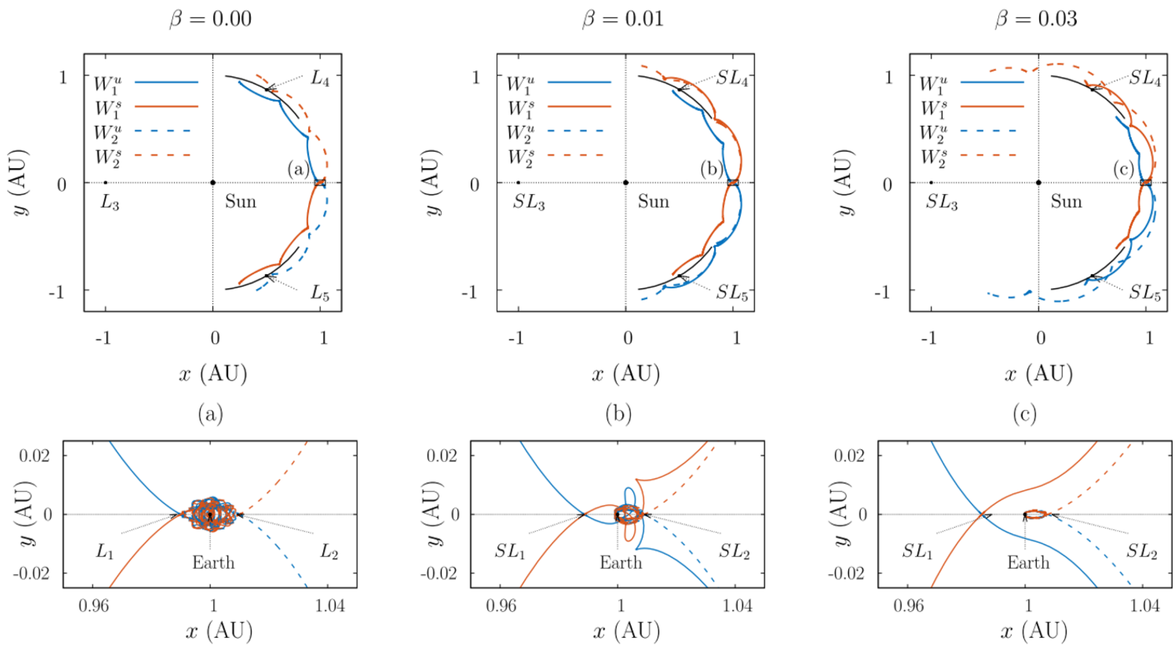

Figure 3.2: Invariant manifolds of the same solar-sail augmented CR3BP from literature [7].

less computationally heavy compared to the trajectory integration done in the initial guess generation, but still show the ability of the algorithm to find a (locally) optimal solution.

The Himmelblau function is a classic optimization algorithm test function, described by

$$f(x, y) = \left(x^2 + y - 11\right)^2 + \left(x + y^2 - 7\right)^2 \tag{3.1}$$

It has four local minima which are given by

$$\begin{aligned} f(3.0, 2.0) &= 0.0 \\ f(-2.805118, 3.131312) &= 0.0 \\ f(-3.779310, -3.283186) &= 0.0 \\ f(3.584428, -1.848126) &= 0.0 \end{aligned} \tag{3.2}$$

The chromosome is then given by

$$\mathbf{g}_h = [\ x \quad y\ ]^T \tag{3.3}$$

The genetic algorithm is able to find three of the four local minima using 10 different seed values. The sphere function is given by

$$f(\mathbf{x}) = \sum_{i=1}^{7} x_i^2 \tag{3.4}$$

with its chromosome

$$\mathbf{g}_s = \mathbf{x} = [x_1, x_2, x_3, x_4, x_5, x_6, x_7] \tag{3.5}$$

It was chosen to see how the genetic algorithm handles a chromosome that is larger than the 2 genes of the Himmelblau function, because the initial guess generation uses a chromosome of length 7. For this test function, the genetic algorithm also finds a solution close to the known local optimum ($x_i = 0$ for $i = 1, 2, 3..., 7$).

The best fitness of the population over the 50 generations is shown in Figure 3.3a and Figure 3.3b, for the Himmelblau function and the sphere function respectively. Both decrease steadily over the generations, indicating that the genetic algorithm is able to converge towards the local optima.

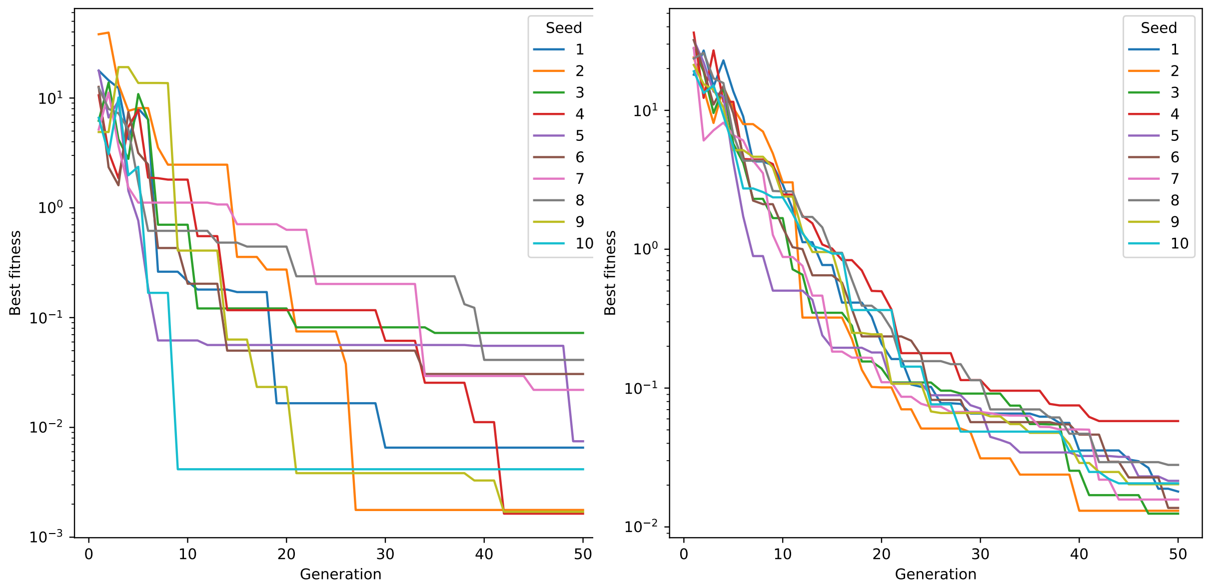

(a) Himmelblau function.

(b) Sphere function.

Figure 3.3: Best fitness in each generation over generations in the genetic algorithm for 10 different seed values for a) the Himmelblau function and b) the sphere function.

3.3. PSOPT Results

The results of PSOPT are verified by reintegrating the initial states of the CR3BP and EH3BP over time with Python's `scipy.integrate.solve_ivp` function using an explicit Runge Kutta method of order 8. These verified results are shown in Figure 3.4. The reintegrated results overlap accurately with the PSOPT results.

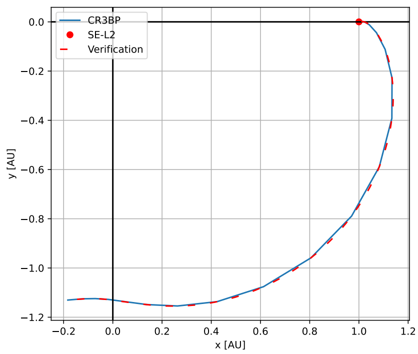

(a) Outbound CR3BP.

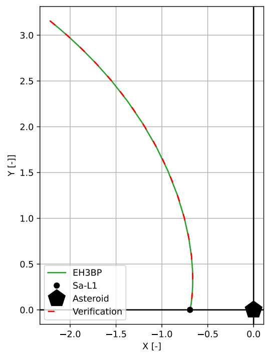

(b) Outbound EH3BP.

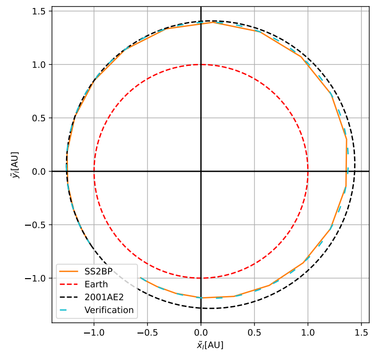

(c) Outbound SS2BP.

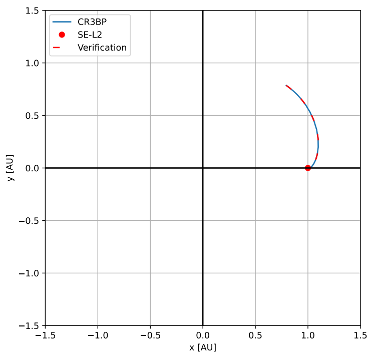

(d) Inbound CR3BP.

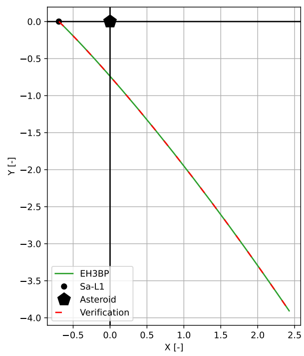

(e) Inbound EH3BP.

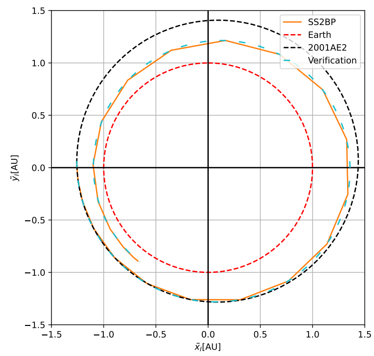

Figure 3.4: Verification of the PSOPT results by reintegration of initial states.

4 Conclusions and Recommendations

Solar sailing is an innovative technique, serving as an effective and sustainable alternative to conventional propulsion methods and exceling in long-duration operations. Solar radiation pressure can steadily increase the velocity of a solar sail to match and exceed velocities achieved through conventional propulsion methods. Furthermore, it's energy source is inexhaustible and constantly available. An interesting use-case for this relatively new technology are cyclers. Future long duration space operations at asteroids, such as asteroid mining or other crewed operations, may require a continuous line of logistical support. Solar sail spacecraft are an outstanding match for this as they do not need fuel to instigate orbital manoeuvres (e.g., guidance corrections), instead relying on the ever-present solar radiation. The solar sail asteroid cycler designed in this work is able to repeatedly visit asteroid 2001AE2.

Inital sub-optimal trajectories with constant sail attitudes in the different phases of the cycle are found using invariant manifolds resulting from the Circular Restricted Three-Body Problem (CR3BP) and the Elliptic Hill (Three-Body) Problem (EH3BP). Using a genetic algorithm to find connections of these manifolds through an intermediate two-body problem (SS2BP) results in initial guess trajectories that can be further optimized in PSOPT. PSOPT uses a pseudospectral collocation method to transform the infinite dimensional control problem (i.e., finding a continuous control profile over time) into a finite dimensional non-linear programming problem. This results in the time-optimal trajectories presented in the article above, which are used for the solar sail asteroid cycler to asteroid 2001AE2.

This chapter concludes the thesis research, answering the research questions and research objective in Section 4.1. Finally, Section 4.2 gives recommendations for future research.

4.1. Review of Research Objective and Questions

The research questions will be answered one by one following with a conclusive answer to the research objective.

To investigate the dynamical model used in proximity of the asteroid, a suitable asteroid has to be selected from a relatively varied set of asteroids in terms of orbital characteristics. Near-Earth asteroids (NEAs) have an orbit that brings them in proximity to Earth, with a perihelion less than 1.3 AU (i.e., at some point their orbit brings them closer to the Sun than Mars)[5]. Other than that, their orbital characteristics (e.g., semi-major axis, eccentricity, and inclination) vary significantly.

Initially, the aim of this work was to set up a general methodology for finding solar sail asteroid cycler trajectories and test this on various asteroids. It would start with an 'easy' to reach target and subsequently apply the same methods to more 'difficult' to reach targets. However, due to time constraints the work was limited to the first target.

This lead to the first research question:

> **What physical characteristics are of consideration when selecting the initial target asteroid and which orbital characteristics distinguish an easy to reach target from a more difficult to reach target?**

Firstly, the availability of asteroid data is important to consider when approaching this question. There is a lot of research being done into asteroids, cataloged in large databases such as JPL's Small-Body

DataBases [16] and the Minor Planet Center [8]. However, there are large gaps in availability and large uncertainties in most values. For instance, of the approximately 30,000 known NEAs (as of 2023), only 326 have a determined spectral type. Although spectral type is an interesting property because it can given an indication of (surface) material, it does not influence the gravitational dynamical models used to determine transfer trajectories (i.e., the CR3BP, SS2BP and EH3BP) and therefore does not qualify an asteroid as being easy or difficult to reach. Hence, it is not a key metric for testing the methodology. Nonetheless, it is still of minor consideration in this work as it can increase capital profitability or scientific interest in the asteroid. Similarly, rotation and shape factors are not included in the target selection as the EH3BP assumes the asteroid's gravitational attraction to function as a point source.

On the other hand, one physical characteristic that is taken into consideration despite sparse availability of data is the diameter of the asteroid as it can be estimated through other observed characteristics of the asteroid. In order to increase capital profitability and scientific interest, an asteroid with a large diameter is preferred in this research. Currently approximately 40% of all discovered NEAs has a diameter of size $D \geq 0.140$km. This is used as one of the thresholds for the selection.

In terms of orbital characteristics, two Kepler elements describing asteroid orbits were found to be of importance: the eccentricity and the inclination. Previous research into cyclers used the synodic period to determine the cycle time [23]. Whereas the synodic period is useful for targets with a circular coplanar orbit, as soon as a body with a highly eccentric or inclined orbit is targeted this timing method is no longer useful. The synodic period results in the same relative position of the two bodies at the end of a cycle, but for highly eccentric or inclined orbits the bodies need to be in the same absolute position with respect to an inertial reference frame. In those cases the mean-motion resonance (MMR) is suggested to be used instead.

To investigate whether the methodology can be used for any NEA regardless of eccentricity and ensure generality, the elliptic Hill problem is used in this work. To emphasize this necessity, note that more than 90% of all NEAs have an eccentricity higher than 0.2. Nonetheless, for the initial target, a nearly circular orbit is preferred so the methodology can also use the synodic period in case there is no asteroid available with a suitable MMR.

Furthermore, almost half of the NEA population has an inclination higher than 10 degrees. For asteroids with a high inclination orbit, the plane changes are very time consuming. Hence, a small inclination is preferable for the initial target for the same reason a (nearly) circular orbit is preferred.

To summarize, at the start of the thesis the aim was to design a cycler for multiple asteroids, to investigate the methodology for the different orbital parameters. To start, an asteroid was to be selected that would be considered 'easily' reachable. Here, 'easy' is found to mean an asteroid that is nearly circular and coplanar with Earth with an orbital period that results in a close MMR with Earth. In order to select a suitable asteroid to demonstrate the method of using heteroclinic-like connections between the Sun-Earth's CR3BP Lagrange point 2 (SE − L2) and the Sun-asteroid EH3BP's Lagrange point 1 (Sa − L1), the following filters and selection criteria are suggested to be used:

1. Filter A: $i \leq 5$deg
2. Filter B: $e \leq 0.1$
3. Filter C: $D \geq 0.140$km

With these considerations, the target asteroid that was selected is asteroid 2001AE2. It was selected because it is in an almost circular ($e = 0.0815$), coplanar ($i = 1.66$deg) orbit, and has a relatively large estimated diameter ($D_{est} = 0.452$km). Finally, its MMR with respect to Earth is close to $n_{ast} : n_{Earth} = 7 : 11$, meaning the asteroid completes 7 revolutions in one cycle whereas Earth completes 11 revolutions in one cycle. There is only a slight delay of approximately 9 days in Earth's position at the end of one cycle. However, with the synodic period ($T_{syn} = 2.760$y) an even better cycle time can be used of $T_{cyc} = 4 \times 2.76 = 11.04$y. This eliminates the position mismatch of the celestial bodies at the end of the cycle, but does require making the assumption of the asteroid orbit being perfectly circular and coplanar with Earth's orbit. In this case, that assumption is justified because the inclination and eccentricity are deliberately selected to be very small.

Furthermore, it is coincidentally a SMASSII T-type asteroid, which indicates a possibly "primitive" composition. For initial asteroid cyclers these types of asteroids can be especially interesting from a scientific perspective, as their primitive composition can be tied to the early Solar System. The D and T classes are of special interest, though they are mostly found in the outer asteroid belt and among Jupiter Trojans [4].

What is the minimum time-of-flight of the transfer trajectories between SE − L2 and Sa − L1 and what are therefore the maximum dwelling times at these points for the solar sail asteroid cycler to the asteroid selected through Research Question Q-1?

With asteroid 2001AE2 selected as the target asteroid, transfer trajectories were searched for using invariant manifold theory [14] and optimization software suite PSOPT [3].

First, an initial guess was generated using a genetic algorithm, by searching for connection points between the invariant manifolds emerging from the CR3BP and the SS2BP-extended EH3BP. This trajectory design assumes a constant sail orientation throughout the two parts of the outbound and inbound trajectory. The algorithm was succesful in finding these sub-optimal trajectories.

Next, these initial guess trajectories were optimized in PSOPT. This resulted in a significant reduction in time, as the sail orientation is allowed to change throughout the trajectories. For asteroid 2001AE2, the resulting initial cycle for the cycler would depart from SE − L2 at 01 − 03 − 2036 and arrive at 2001AE2's

$$\mathrm{Sa} - \mathrm{L1}$$

point at 02 − 04 − 2039.

The minimum time of flight found by PSOPT for the outbound trajectory is 1127 days. For the inbound trajectory, this is only 969 days. These times of flight assume near-future sail technology with a lightness number of $\beta = 0.05$.

It is available at Sa − L1 for 4.34 years, to perform mission operations until its departure from the asteroid at 04 − 08 − 2043. Finally it would return to SE − L2 at 31 − 03 − 2046. The subsequent cycle would start 351 days later.

These dwelling times are very long, especially Sa − L1. This is not necessarily a negative outcome. If the focus of the cycler is solely to (un)load its payload as fast as possible and continue with its cycle, then a shorter dwelling time might be preferable. But for an initial cycler, scientific interest is still important and these long dwelling times can be used for research purposes.

What is the quality of the heteroclinic-like connections found between SE − L2 and Sa − L1 of the target asteroid that was selected in Research Question Q-1?

The discontinuities at the connection points are on the order of 10^4km for the position vectors and on the order of 10^{-2}km/s or smaller for the velocity vectors. However, because of the significant difference in the time and length scales of the CR3BP and EH3BP, these discontinuities are much larger in the non-dimensional units of the EH3BP (on the order of $\tilde{1}0^2$) than in the non-dimensional units of the CR3BP (on the order of 10^{-4}). Since the connection point of the asteroid is much closer to the asteroid (up to a few hundred kilometers from the asteroid), a position mismatch on the order of thousands of kilometers is also a lot more significant. However, as mentioned before, the dwelling time at Sa − L1 is relatively long and can be used in future studies to refine the connection between the EH3BP and the SS2BP for both the outbound and inbound trajectories. Furthermore, it is important to recall that an increase of ≈ 10% can be expected when using non-ideal sail models, based on the results of Reference [23], which will also decrease the dwelling times.

It is clear, though, that the optimization scheme as it is currently set up has difficulty decreasing the non-dimensional size of the discontinuity at these connection points. Further research is recommended to investigate the use of the EH3BP, especially the connection of its invariant manifolds to the SS2BP or potentially directly to the Sun-Earth CR3BP.

To conclude, the research objective is revisited.

Can a heteroclinic-like connection be found between the SE − L2 point and the Sa − L1 point of a suitable asteroid to demonstrate the feasibility of setting up a solar sail Earth-asteroid cycler?

There are still discontinuities of considerable order for the connection between the intermediate SS2BP and the EH3BP phases. Future work is needed to further optimize the results, but taking into account the assumptions addressed throughout this work and noting that these methods serve as an preliminary trajectory design, the methodology used in this work shows clear potential for solar sail asteroid cyclers set up through heteroclinic-like connections of the Sun-Earth CR3BP and the Sun-asteroid EH3BP. With that, the research objective is believed to be met.

4.2. Recommendations

The results from this thesis showcase a clear potential for solar sail Earth-asteroid cyclers. The elliptic Hill problem has been tested for an asteroid with a circular orbit and a methodology has been suggested for determining a suitable cycler time based on the MMR instead of the synodic period. Future work is recommended to investigate whether this cyler design also works for asteroids in an orbit with a high eccentricity or inclination.

It is important to note that this work makes use of assumptions and simplifications so the results should be interpreted as serving as an initial proof of concept for a solar sail asteroid cycler and not as a finalized set of trajectories. Currently, the spacecraft is assumed to be stationary at $SE-L2$ and $Sa-L1$ during the dwelling times, but in practice this is unrealistic. Rather, libration point orbits should be included in the design to fill the dwelling time of the cycle. The CR3BP is an often used model in preliminary trajectory design, but on its own it disregards the gravitational influence of other celestial bodies acting on the spacecraft. Furthermore, simple two-body dynamics are used to model the trajectory in between the CR3BP and the EH3BP. Gravitational influence of other celestial bodies is not incorporated, such as the other inner planets and Jupiter. Future work is also needed to include higher fidelity models for the spacecraft dynamics in close proximity to the asteroid, such as the rotation and shape of the asteroid.

Future work is recommended to investigate varying the lightness number, to see how much the lightness number (in other words, the mass-to-area ratio) can be decreased while still finding trajectories that fit within the cycle time. That can eventually help estimate how much the payload can be increased, which is a key mission design characteristic.

Perhaps the most important next step is to recalculate the trajectories using optical or parametric sail models, to account for non-ideal properties of the sail. Non-perfect reflectivity due to absorption and re-radiation, as well as billowing of the sail both have significant impact on the time of flight.

References

[1] E E Aldrin. *Cyclic Trajectory Concepts*. 1985.

[2] Viorel Badescu. *Asteroids Prospective Energy and Material Resources*. Springer, 2013. ISBN: 978-3-642-39243-6. DOI: 10.1007/978-3-642-39244-3.

[3] Victor M. Becerra. *PSOPT*. 2009. URL: https://github.com/PSOPT/psopt.

[4] Richard P. Binzel et al. "Dynamical and compositional assessment of near-Earth object mission targets". In: *Meteoritics and Planetary Science* 39.3 (2004), pp. 351–366. ISSN: 10869379. DOI: 10.1111/j.1945-5100.2004.tb00098.x.

[5] ESA and Karel A. van der Hucht. *NEO Chronology*. 2023. URL: http://neo.ssa.esa.int/neo-chronology (visited on 12/04/2020).

[6] A Farrés and Angel Jorba. "Orbital Dynamics of a Solar Sail Near L1 and L2 in the Elliptic Hill Problem". In: *Proceedings of 63rd International Astronautical Congress*. 2012.

[7] Ariadna Farrés, Jeannette Heiligers, and Narcís Miguel. "Road map to L4/L5 with a solar sail". In: *Aerospace Science and Technology* 95 (2019), p. 105458. ISSN: 12709638. DOI: 10.1016/j.ast.2019.105458. URL: https://doi.org/10.1016/j.ast.2019.105458.

[8] J.L. Galache. *Guide to the Extended Versions of MPC Data Files Based on the MPCORB Format*. 2016. URL: https://minorplanetcenter.net/Extended{_}Files/Extended{_}MPCORB{_}Data{_}Format{_}Manual.pdf (visited on 12/08/2020).

[9] Michael Greshko. *NASA's OSIRIS-REx secures asteroid sample after surprise leak*. 2020. URL: https://www.nationalgeographic.com/science/article/nasa-osiris-rex-secures-asteroid-sample-after-leak-bennu.

[10] Walter M Hollister. "Periodic orbits for interplanetary flight." In: *Journal of Spacecraft and Rockets* 6.4 (1969), pp. 366–369. DOI: https://doi.org/10.2514/3.29664.

[11] Les Johnson et al. "Status of solar sail technology within NASA". In: *Advances in Space Research* 48.11 (2011), pp. 1687–1694. ISSN: 02731177. DOI: 10.1016/j.asr.2010.12.011. URL: http://dx.doi.org/10.1016/j.asr.2010.12.011.

[12] Kyodo. *Hayabusa2 returned with 5 grams of asteroid soil, far more than target*. 2020. URL: https://www.japantimes.co.jp/news/2020/12/19/national/science-health/hayabusa2-asteroid-soil/.

[13] Colin R. McInnes. *Solar Sailing Technology, Dynamics and Mission Applications*. Springer-Verlag, 1999. ISBN: 978-1-85233-102-3.

[14] Giorgio Mingotti, Jeannette Heiligers, and Colin McInnes. "First-guess generation of solar sail interplanetary heteroclinic connections". In: *Advances in the Astronautical Sciences* 153 (2015), pp. 1633–1651. ISSN: 00653438.

[15] Osamu Mori et al. "Overview of IKAROS Mission". In: *Advances in Solar Sailing*. Ed. by Malcolm Macdonald. Springer Berlin Heidelberg, 2014, pp. 25–43. ISBN: 978-3-642-34907-2. DOI: 10.1007/978-3-642-34907-2_3.

[16] NASA/JPL CNEOS. *NASA/JPL Small Body Database*. 2023. URL: https://ssd.jpl.nasa.gov/?tools (visited on 12/04/2020).

[17] Jeffrey S. Parker. "Low-Energy Ballistic Lunar Transfers". PhD thesis. 2007. URL: http://ccar.colorado.edu/geryon/papers/Misc/Parker{_}Thesis.pdf.

[18] L Prockter et al. "The NEAR Shoemaker mission to asteroid 433 Eros". In: *Acta Astronautica* 51.1 (2002), pp. 491–500.

[19] D. J. Scheeres and F. Marzari. "Spacecraft dynamics in the vicinity of a comet". In: *Journal of the Astronautical Sciences* 50.1 (2003), pp. 35–52. ISSN: 00219142. DOI: 10.1007/bf03546329.

[20] Daniel J. Scheeres. *Orbital Motion in Strongly Perturbed Environments; Applications to Asteroid, Comet and Planetary Satellite Orbiters*. Springer-Verlag Berlin Heidelberg, 2012. ISBN: 9783642032554. DOI: 10.1007/978-3-642-03256-1.

[21] David A Spencer et al. "The LightSail 2 solar sailing technology demonstration". In: *Advances in Space Research* (2020). DOI: 10.1016/j.asr.2020.06.029.

[22] Victor Szebehely. *Theory of orbits*. 1967.

[23] Merel Vergaaij and Jeannette Heiligers. "Time-optimal solar sail heteroclinic-like connections for an Earth-Mars cycler". In: *Acta Astronautica* 152.August (2018), pp. 474–485. ISSN: 00945765. DOI: 10.1016/j.actaastro.2018.08.008.

[24] Karel F. Wakker. *Fundamentals of Astrodynamics*. Delft University of Technology, 2015. ISBN: 9789461864192.